PCCP

Synthesis, Properties, and Formation Mechanism of Mn-doped Zn2SiO4 nanowires and Associated Heterostructures

SCHOLARONE™
Manuscripts

Synthesis, Properties, and Formation Mechanism of Mn-doped Zn_2SiO_4 nanowires and Associated Heterostructures

Haiqing Liu,[a] Dominic Moronta,[a] Luyao Li,[a] Shiyu Yue,[a] and Stanislaus S. Wong[a,*]

[a]Department of Chemistry, State University of New York at Stony Brook, Stony Brook, NY 11794-3400, USA

*To whom correspondence should be addressed. Phone: 631-632-1703; 631-344-3178
Email: Stanislaus.wong@stonybrook.edu; sswong@bnl.gov

Abstract: In this work, we have put forth a facile hydrothermal approach to synthesize an array of one-dimensional (1D) Mn-doped Zn_2SiO_4 nanostructures. Specifically, we have probed and correlated the effects of controllable reaction parameters such as the pH and Mn dopant concentrations with the resulting crystal structures and morphologies of the products obtained. Based upon our results, we find that careful tuning of the pH versus the Mn dopant level gives rise to opposite trends with respect to the overall size of the resulting one-dimensional nanostructures. Significantly, we have highlighted the role of the Mn dopant ion concentration as a potentially generalizable reaction parameter in solution-based synthesis for controlling morphology and hence, the observed optical behavior. Indeed, such a strategy can be potentially generalized to systems such as but not limited to Mn-doped ZnS, CdS, and CdSe quantum dots (QD), which, to the best of our knowledge, denote promising candidates for a variety of optoelectronic applications. Specifically, we have carefully optimized the synthesis conditions in order to generate a series of chemically well-defined Mn-doped Zn_2SiO_4 not only possessing Mn concentrations ranging from 3% to 8% but also characterized by highly crystalline, monodisperse wire-like motifs measuring ~30 nm in diameter and ~ 700 nm in length. Optically, the photoluminescence signals associated with the 1D series yielded a volcano-shaped relationship between PL intensities and the Mn dopant level. In additional experiments, we have immobilized CdSe quantum dots (QDs) onto the external surfaces of our as-synthesized Mn-doped Zn_2SiO_4 nanowires, in order to form novel composite heterostructures. The optical properties of the CdSe QD - Mn: Zn_2SiO_4 heterostructures have been subsequently examined. Our results have demonstrated the likely co-existence of both energy transfer and charge transfer phenomena between the two constituent components of our as-prepared composites. Specifically, when both components are photoexcited, both energy transfer and charge transfer were found to plausibly occur, albeit in opposite directions. When the CdSe QDs are excited alone for example, charge transfer probably takes place from the CdSe QDs to the dopant Mn^{2+} ions. We believe that our as-processed heterostructures are therefore promising as a tunable light-harvesting motif. Essentially, these materials have broadened the effective light absorption range for optical 'accessibility', not only through their incorporation of dopant-tunable Zn_2SiO_4 possessing complementary absorption properties to those of the QDs but also through their integration of CdSe QDs with size-tailorable optical behavior.

Keywords: zinc silicate, nanowires, CdSe quantum dots, heterostructures, energy transfer, charge transfer

1. Introduction

As a viable phosphor, the observed color emission of Zn_2SiO_4 can be tuned by the nature and amount of dopant integrated into it. Specifically, Mn-doped zinc silicate (Zn_2SiO_4: Mn^{2+}) has been incorporated as a key element of fluorescent lamps, neon discharge lamps, oscilloscopes, black-and-white televisions, color televisions, and many other displays and lighting devices,[1] respectively, due to its long lifetime, which is of significant importance in minimizing the degree of flicker within displays.[2] Many reports have investigated the relationship between the quantitative Mn dopant level and the corresponding photoluminescent (PL) signal, with the ideal Mn concentration found to range from 1% to 4% for bulk materials and nanoparticles, depending upon the synthetic approaches used.[3, 4]

Nonetheless, we observe that there have been very few studies correlating the preparative synthesis method with the resulting morphology of such nanoscale Zn_2SiO_4 materials. That is, there has yet to be a rational mechanistic understanding of how to controllably generate, for instance, (a) one-dimensional (1D) nanowires and nanotubes and/or (b) three-dimensional (3D) motifs, associated with these precise chemical compositions.[5] In the context of optical properties, one-dimensional (1D) structures provide for fewer defects, which minimize trap sites on the surface that are detrimental to excitons, as compared with their 0D (i.e. nanoparticles) counterparts.[6, 7] To date, a number of gas-phase and/or instrumentation-intensive protocols including but not limited to silicon etching,[8] chemical vapor deposition (CVD),[9, 10] vapor–liquid–solid (VLS),[11] and electrospinning[12] have been used to yield either highly-aligned 1D nanowire or 3D nanowire bundle arrays of Zn_2SiO_4.

In recent years, many groups have reported upon potentially more straightforward, solution-based (especially hydrothermal-inspired) synthetic approaches to generate either

Physical Chemistry Chemical Physics

micron-sized wires,[13] nanorods,[14, 15] or 3D spindle-like[16] structures. However, the size distributions of most of these materials tend to be generally rather large and polydisperse. In addition, only very few of these procedures have demonstrated a capability for producing Mn-doped Zn_2SiO_4 without loss of control over the resulting 1D morphology.[15, 17] In order to address this problem of ensuring reasonable chemical, size, and morphological uniformity, we have experimentally determined herein that varying the dopant level itself as an *independent and tailorable* synthetic parameter can substantively affect the resulting detected morphology, i.e. size and shape, and hence, the corresponding optical properties observed. That is, we are among the first to have demonstrated the viability of rationally altering dopant ion concentration as a deliberate means of controlling nanoscale morphology, especially in the context of one-dimensional materials. We note that this is a fundamentally generalizable solution-based strategy, that can be applied to the synthesis of *all* types of nanomaterials.

As a separate issue, there has been an increasing level of interest in combining various types of distinctive nanoscale motifs within the context of multi-functional nanoscale hybrids or heterostructures. For instance, Wang *et al.* have demonstrated the synthesis of Zn_2SiO_4-SiO_x hybrid nanowires, possessing average lengths of 800 nm and diameters of 20 nm, grown onto and emanating from a Si substrate.[18] Overall, these heterostructures exhibited dichromatic emission with peaks located at both 404 nm and 521 nm, which could be attributed to SiO_2 and Zn_2SiO_4, respectively. In addition, Zhou *et al.* fabricated Zn_2SiO_4 nanotube / ZnO nanowire heterojunction arrays by using ZnO nanowire arrays as the template; these unique structures gave rise to an additional emission band centered at ~523 nm, associated with Zn_2SiO_4, in addition to the expected contribution from pure ZnO.[19] Recently, Kwon *et al.* have reported the preparation of a core/shell SiO_2/Zn_2SiO_4: Mn^{2+} composite structure, generated through a thermal-diffusion

reaction involving SiO_2 and $Zn_{1-x}Mn_xO$ particles.[20] From a photophysics perspective, this architecture exhibited a shorter decay time as compared with that of conventional Zn_2SiO_4: Mn^{2+} particles.

Nevertheless, in these prior reports, the observed emission of these heterostructures was attributed primarily to a linear superposition and combination of the optical signals, associated with the individual component subunits. Because these studies were mainly phenomenological in nature, no evidence was provided to either prove or disprove any plausible optoelectronic effects, such as but not limited to Förster resonance energy transfer (FRET) and / or other types of non-radiative optical transitions and recombination processes that might have been occurring between the adjacent, constituent components within the heterojunctions themselves.

As a matter of principle, our group has subscribed to the idea that the whole is often greater than the sum of the individual constituent parts and that favorable, synergistic interactions between the different elements within these heterostructures can give rise to overall more desirable and appealing properties as compared with those associated with their separate and discrete components. As such, throughout the years, we have been aiming to probe and understand the inherent nature of nanoscale heterostructures, namely the interfaces between 0D quantum dots and 1D phosphors. Specifically, we have done so by coupling quantum dots with a variety of different and distinctive 1D systems, including carbon nanotubes and metal oxides.[21]

For example, our recent body of work on CdSe QD-CNT heterostructures combined NEXAFS, Raman, and electron transport studies with theory in order to shed light on the electron dynamics within this hierarchical architecture, i.e. QDs immobilized onto a 1D motif. Our efforts sought to analyze and understand charge and energy transfer processes as a specific

function of (a) the QD size, (b) the chemical identity connecting the QD with the carbon

nanotube, as well as (c) the QD coverage density onto the underlying carbon nanotube itself.[22, 23]

Additionally, our work on cerium phosphate ($CePO_4$)-based QD heterostructures

highlighted that the optical properties of such systems can be tailored by engineering the band

gaps and relative band gap alignments of the constituent components so as to favor charge

separation.[24] The study of lanthanum phosphate ($LaPO_4$)-based QD heterostructures was

motivated by a desire to understand the role of the metal oxide substrate morphology,

specifically comparing and contrasting the use of a 1D versus a 3D structure. Indeed, the choice

of morphology could actually favor the predominance of energy versus charge transfer processes

or vice versa.[25] Furthermore, we observed composition-modulated luminescence in our

systematic study of molybdate and tungstate-based QD heterostructures, definitively showing

that optical properties of composite heterostructures could be chemically tuned to a surprising

degree by altering the chemical signature of either the QDs themselves or of the metal oxide

species.[26] These examples highlight the realistic potential to design and tailor optical properties,

including plausible charge and energy transfer between the two components, within carefully

engineered heterostructures.

To the best of our knowledge, there have *not* been any reports of heterostructures

composed of CdSe QDs coupled with and immobilized onto underlying Zn_2SiO_4 nanowires.

Therefore, concerning the novelty in our current study, we aim to demonstrate precise and

simultaneous control over chemical composition, bandgap engineering, and morphology within

hierarchical systems in order to study possible charge and energy processes within a unique

family of Zn_2SiO_4: Mn / CdSe QD heterostructures.

We should note that zinc silicate is an ideal host material, because its wide bandgap (5.5 eV)[27] enables one to tune optical properties either by doping with ions or coupling its surface with semiconductors possessing relatively comparable energy band levels, i.e. CdSe quantum dots. Moreover, due to this wide bandgap range, we can expect potential chemical stability and optical transparency within the entire UV-visible range.[28] Furthermore, we anticipate that our efforts will permit us to generate 1D semiconducting motifs with a more effective continuous and direct pathway for the electrons to travel.[29] Thus, our primary motivation and expectation of this study is to understand the fundamental optoelectronic interactions within Mn-doped Zn_2SiO_4 - CdSe QD composite systems to the extent that this knowledge becomes useful for the possible incorporation of these heterostructures within higher-performing solar cell configurations.

In this study therefore, we have sought to achieve two separate but equally important objectives. *First*, we aim to synthesize homogeneous, relatively monodisperse one-dimensional Mn-doped Zn_2SiO_4 nanowires possessing a well-defined morphology and incorporating systematically varying Mn dopant concentrations, i.e. using dopant levels to purposely induce the formation of desired morphologies. In particular, we have demonstrated that rational variations in reaction parameters including the pH value and the Mn dopant level can significantly impact upon the observed crystalline structure as well as the morphologies of the resulting materials.

Moreover, we have carefully optimized the synthesis conditions, including the Mn dopant level, in order to generate samples with precise chemical composition. To this end, we have produced a series of highly crystalline and monodisperse Mn-doped Zn_2SiO_4 anisotropic nanowires with average diameters of ~ 30 nm and lengths of ~ 700 nm and with the Mn concentrations spanning a range from 3% to 8%.

Second, we have fabricated, for the very first time, a family of CdSe QD - Mn: Zn_2SiO_4 0D-1D heterostructures. The optical properties of our as-prepared CdSe QD - Mn: Zn_2SiO_4 heterostructures have suggested the possible co-existence and tunability of both energy transfer and charge transfer behavior occurring between the two nanoscale constituent components. We believe that our observations strongly imply that our as-processed composite structures can be viably considered as potentially promising light-harvesting motifs.

2. Experimental

2.1. Materials and Reagents.

We utilized zinc nitrate (99.0%, Baker & Adamson), manganese (II) nitrate tetrahydrate (98.0%, Alfa Aesar), fumed silica (average particle size of ~7 nm, Aldrich), sodium hydroxide (99%, EMD Industries), cadmium oxide (99%, Acros Organics), stearic acid (97%, Acros Organics), selenium (99.5+%, Aldrich), trioctylphosphine oxide (99%, Acros Organics), tributylphosphine (95%, Alfa Aesar), hexadecylamine (90%, Acros Organics), dioctylamine (97%, Acros Organics), and 3-mercaptopropionoic acid (99+%, Acros Organics) as reagents without additional purification.

2.2 Preparation of Mn-doped Zn_2SiO_4 nanowires

We have adopted but modified a hydrothermal method from a previous report in order to generate monodisperse Mn-doped Zn_2SiO_4.[13] In so doing, for the first time, we have highlighted and targeted the specific roles of pH and Mn dopant concentration in controlling the growth of uniform and homogeneous wires of this particular material. Specifically, for the synthesis of pure Zn_2SiO_4, 3.2 mmol of $Zn(NO_3)_2$, 1.6 mmol of fumed SiO_2, and 8 mL of de-ionized water were placed within a 25 mL Teflon holder. 2 M sodium hydroxide (NaOH) was subsequently added to

the Teflon cup in order to adjust the pH to a desired value, i.e., a range of 10-13, followed by stirring for 10 minutes. The Teflon cup containing the reagents was then transferred into the metal autoclave, and later heated to 220°C for 24 h. Once the reaction was complete, the sample was collected, centrifuged, and twice washed, prior to drying overnight at 80°C.

Separately, in order to synthesize Mn-doped Zn_2SiO_4 samples, varying amounts of $Mn(NO_3)_2$ systematically ranging from 0 to 10% with respect to $Zn(NO_3)_2$, corresponding to a Mn dopant concentration extending from 0 to 0.32 mmol, were added to the reaction mixture, described above. All of the other reaction parameters were kept constant in these protocols.

2.3. Synthesis of CdSe quantum dots and fabrication of Mn: Zn_2SiO_4 – QD heterostructures

2.3.1. Quantum Dot (QD) Synthesis

The synthesis preparation protocol of CdSe QDs was modified from an existing literature procedure.[30] Briefly, 0.2 mmol of CdO and 0.8 mmol of stearic acid were added to a three-necked round bottom flask, then degassed, and ultimately heated at 150°C under an Ar atmosphere. Once the contents were dissolved, 3.88 g each of trioctylphosphine oxide (TOPO) and hexadecylamine (HDA) were added to the flask and heated to 320°C. Separately, a precursor selenium (Se) solution was prepared in an air-sensitive glovebox environment, wherein the Se was dissolved in tributylphosphine (TBP) and dioctylamine (DOA). Once the solution mixture had reached a temperature of 320°C within the flask, the Se precursor was injected therein, and QD growth was allowed to proceed for 8 minutes at 270°C. After the desired level of growth was attained, the mixture was later cooled to room temperature, then washed with either methanol (MeOH, HPLC Grade 99.9%, Acros Organics) or acetone (ACS grade, 99.5+%), and ultimately stored in hexane.

2.3.2. Ligand Exchange of QDs & Subsequent Formation of QD - Zn_2SiO_4 Heterostructures

CdSe QDs capped with 3-mercaptopropionoic acid (MPA) were synthesized via a ligand exchange reaction. In a typical experiment, a solution of MPA (1 mmol) in 2 mL of MeOH was added to a suspension of as-prepared, capped CdSe QDs (0.04 mmol) in 4 mL of hexane. After stirring for 10 min, the QDs were allowed to visibly precipitate upon ligand exchange. These QDs were later collected by centrifugation and then washed with aliquots of both ethanol and MeOH. The resulting QDs were finally re-dispersed in MeOH for further characterization.

Subsequently, MPA-capped CdSe QDs were attached onto as-generated Mn-doped Zn_2SiO_4 nanowires. This interaction occurred presumably through a hydrogen bonding mechanism involving the mediation of hydroxyl and acid-based groups of MPA, adsorbed onto the external, heavily oxygenated surfaces of Zn_2SiO_4. This strategy was similar to the protocols that we had previously reported and successfully used in prior reports associated with the attachment and immobilization of CdSe QDs onto the external surfaces of various types and motifs of metal oxide species, including (i) $CePO_4$: Tb nanowires, (ii) 1D nanowires and sea-urchin-like 3D nanostructures of $LaPO_4$: RE (RE = Eu, Ce, and Tb), (iii) $CaWO_4$ nanowires, (iv) $CaMoO_4$-$CaWO_4$: Eu^{3+} nanowires, as well as (v) sub-micron sized $CaTiO_3$-based spherical assemblies.[21, 24-26, 31]

For example, in a typical experiment, 2.3 mg (10.4 μmol) of Mn: Zn_2SiO_4 nanowires in 2 ml MeOH was added to 2 mg (10.4 μmol) of MPA-capped CdSe QDs in 2 mL of MeOH. The resulting solution was subsequently sonicated and stirred in the dark for 30 min, so as to preserve optical integrity. These as-prepared heterostructures, which had been dispersed in MeOH, were then used for further characterization and analysis.

2.4. Structural and Optical Characterization (XRD, TEM (EDAX), XPS, PL (Lifetime))

2.4.1. X-ray Diffraction (XRD)

The crystallographic purity of (i) as-prepared pure as well as of (ii) Mn-doped Zn_2SiO_4 was confirmed using powder XRD. Diffraction patterns were obtained using the Rigaku Miniflex diffractometer. This instrument was operated in the Bragg configuration using Cu Kα radiation (1.54 Å), and data were collected as a function of varying 2θ lattice parameters, ranging from 10 to 80°, obtained at a scanning rate of 1.0°/min for all of the samples, synthesized herein.

2.4.2. Electron Microscopy

Transmission electron microscopy (TEM) was employed. Specifically, we collected samples at an accelerating voltage of 120 kV with the JEOL JEM-1400 instrument, equipped not only with a 2048 x 2048 Gatan CCD digital camera but also with energy dispersive spectroscopy (EDS) mapping capabilities. High-resolution (HRTEM) images along with selected area electron diffraction (SAED) patterns were obtained using the JEOL 2100 microscope, which had been set at an accelerating voltage of 200 kV. Sample preparation protocols for microscopy analysis involved the use of an ethanolic dispersion followed by sonication. Subsequently, the solution was deposited dropwise onto a lacey carbon film-coated 300 mesh Cu grid. When measuring the lengths and diameters of each of our nanoscale samples analyzed, at least 50 different measurements on expected, targeted features (whether they be quantum dots, nanowires, or heterostructures) were obtained over a minimum of at least 10 different TEM images of the same sample. Hence, the values reported in the Results and Discussion section denote a representative average of the corresponding data points collected.

2.4.3. X-ray photoelectron spectroscopy measurements

As-prepared Mn doped Zn_2SiO_4 nanorods were initially dispersed in ethanol and small aliquots of that solution were spread, i.e. drip cast, onto a Si wafer (measuring 1 cm × 1 cm),

followed by evaporative drying in air. XPS spectra were collected by irradiating with a Mg Kα

X-ray source (hυ = 1253.6 eV) (model XR 50) operating under current—voltage conditions of 30

mA and 13 kV. The angle between the analyzer and the X-ray source was set at 45°.

Photoelectrons were captured along the sample's surface normal vector. The curve fitting

algorithm was performed using commercial Casaxps software, and the final processed data were

plotted using the corresponding Origin software.

2.4.4. UV-visible and fluorescence spectroscopy.

In both the UV-visible and fluorescence experiments we performed, all sample solutions

were processed and measured with a concentration of 5 μmol/mL in order to ensure adequacy of

data comparison. All of the UV-visible spectra, including that collected on both bare and MPA

capped CdSe QDs, Mn-doped Zn_2SiO_4 nanostructures, as well as MPA-capped CdSe QD –Mn-

doped Zn_2SiO_4 heterostructures were collected at high resolution with a ThermoSpectronics UV1

spectrometer using quartz cells, possessing a 10 mm path length. The corresponding fluorescence

data were subsequently obtained at room temperature using a FluoroMax-4 spectrofluorimeter

(Jobin Yvon) with 5 s integration times, and acquired at excitation wavelengths of 265 nm and

388 nm, respectively. We note that the fluorescence intensity units used in all of the relevant

plots presented herein refer to the number of photons detected (i.e., counts). Additional

fluorescence lifetimes were measured with a FluoroMax-4 spectrofluorimeter, equipped with two

different sets of IBH NanoLEDs (emitting at 270 nm and 388 nm, respectively) as the excitation

source, and a NanoLED controller module, Fluorohub (Jobin Yvon), operating at 1 MHz. The

decay data analysis was put together using the results, achieved with the mediation of the DAS6

software (Horiba Jobin Yvon IBH). Both the fluorescence experiments and lifetime

measurements were conducted for a minimum of three times to ensure reproducibility. Error bars,

representing calculated standard deviations, have been included in all relevant plots and tables.

3. Results and Discussion

3.1. Mn dopant ion concentration dependence on formation and growth of Mn-doped Zn$_2$SiO$_4$ nanowires

First, we have synthesized Mn-doped Zn$_2$SiO$_4$ nanowires, possessing various Mn

concentrations. In this section, we chose to use a constant pH value of 12 for the entire series of

samples formed. In so doing, we systematically altered the Mn dopant level within the range of

0% to 10%, so as to probe the potential effect of Mn concentration upon the resulting chemical

compositions, crystal structures, and morphologies of our as-obtained samples.

The XRD patterns are included in Figure 1. As indicated by XRD results, all of the peaks

in most of the as-prepared nanowires can be assigned to a single-crystalline willemite structure

(JCPDS #37-1485), with the exception of the 10% Mn-doped sample. Indeed, the peaks at 29.4°,

32.9°, as well as 36.3° can be indexed to the (112), (103), and (211) planes, respectively, of the

tetragonal ZnMn$_2$O$_4$ crystal structure (JCPDS #71-2499). Therefore, based upon the XRD

pattern, we have calculated the relative molar percentages of Zn$_2$SiO$_4$ and ZnMn$_2$O$_4$ to be 73%

and 27%, respectively.

The fact that such an impurity was found to exist only in the high-Mn concentration

sample is not surprising. As a matter of fact, similar observations have been made previously

with respect to analogous sol-gel synthesis-based Zn$_2$SiO$_4$ nanoparticles.[32] In particular, a

Mn$_2$O$_4{}^{2-}$ complex could potentially form in addition to SiO$_4{}^{4-}$ when the concentration of Mn

exceeds a level of 2%. In effect, that Mn-based complex becomes dominant when either (1) the reaction temperature exceeds 500°C or (2) the Mn dopant level is 10% or higher.[32, 33]

The TEM images of an as-prepared series of Zn_2SiO_4 nanowires incorporating Mn dopant levels ranging from 0% to 10% are shown in Figure 2. The corresponding morphologies as well as the measured dimensions of these samples are summarized in Table 1. Interestingly, we have observed a linear correlation between the overall dimensions of these nanowires and their corresponding Mn dopant percentages. Indeed, as the Mn concentration *increases*, the observed diameters and lengths of the nanowires both *decreased* drastically. Specifically, whereas the 2% Mn-doped Zn_2SiO_4 nanowires maintained diameters of 343 ± 91 nm and lengths of 7.3 ± 1.7 μm, the 4% Mn-doped sample yielded diameters of 29 ± 5 nm and lengths of 627 ± 82 nm. Furthermore, the 6%, 8%, and 10% Mn-doped samples have all exhibited similar anisotropic and unique nanopillar-shaped morphologies, characterized by smaller aspect ratios, in particular with diameters of ~30-40 nm and lengths of ~50-100 nm.

Such a transition to smaller sizes is believed to originate from the incorporation of Mn cations within the Zn_2SiO_4 lattice, since corresponding tensile strains would expect to be noted upon dopant introduction. We should note that very few reports have observed the key role of dopant in determining and dictating morphology. Indeed, a 'dopant-level dependent' morphology has rarely been observed in the literature, especially with respect to solution-based methods. Therefore, we are not certain as to how 'sensitive' the crystal structure actually is towards this sort of imposed strain within the underlying lattice. For instance, it is entirely possible that within the 4-10% doping range, the strain is below a threshold level such that the overall morphology remains relatively the same. Moreover, it is also possible that the *c*-axis is more

sensitive to the dopant-induced strain than either the *a* or the *b* axis, due to the presence of anisotropy within the underlying hexagonal crystal structure.

The influence of the dopant size upon the resulting host size has been previously reported in analogous systems, such as Mn-doped $CdMoO_4$ nanoparticles[34] and Gd-doped $NaYF_4$ nanorods.[35] Specifically, the structural strain caused by the presence of relatively larger dopant ions is expected to give rise to a reduction in either crystallite domain sizes within thin films or in the overall dimensions, i.e. diameters and lengths, of the host nanomaterials; smaller dopant ions by contrast would lead to increases in the relevant dimensions.[34, 36, 37] In addition, an elevated amount of dopant will strengthen and accentuate the magnitude of this phenomenon.[36] Herein, in this system, the ionic radius of Mn^{2+} is 0.83 Å, whereas that of Zn^{2+} is 0.74 Å, thereby explaining the reduction in size upon doping with greater quantities of Mn cations.[38]

The EDS elemental mapping images are presented in Figure S1, and are indicative of a homogeneous distribution of Mn dopant ions within the as-synthesized Zn_2SiO_4 nanostructures, throughout the entire series of as-prepared samples. Moreover, based upon the quantitative EDS results, we have been able to demonstrate that the actual Mn concentrations (normalized to the Zn content) for most of the nanowire samples correlate well with the anticipated values.

Indeed, the dopant levels for the 2%, 4%, 6%, and 8% Mn-doped samples are 1.3% ± 0.7, 3.3% ± 0.9, 5.3% ± 0.9, and 7.2% ± 1.1, respectively. These values are not necessarily 'absolute' quantities, but do nonetheless provide for a very good approximation of the relative amounts of Mn versus Zn in each of the samples tested. Hence, for the sake of simplicity, we have continued to refer to the integral values of the intended dopant levels. We should note that the 10% Mn-doped sample deviates to some extent from this trend, as it yielded an overall Mn dopant level of 7.3% ± 0.9. This observation likely originates from the concomitant formation of $ZnMn_2O_4$,

which effectively lowered the actual incorporation of Mn into the underlying lattice of Zn_2SiO_4.
However, we were unable to detect any different and distinctively novel morphologies within the
10% Mn-doped sample. Our tentative hypothesis is that the $ZnMn_2O_4$ could have formed as an
identical shape to that of Zn_2SiO_4, and that the particular area in which our elemental data had
been collected may have exclusively consisted of Mn-doped Zn_2SiO_4 nanowires.

3.2. pH dependence on formation and growth of Mn-doped Zn_2SiO_4 nanowires

We have also investigated the role of pH. Specifically, we varied the NaOH
concentration, whilst maintaining the rest of experimental parameters as identical. We probed
4% Mn-doped Zn_2SiO_4 as the desired chemical composition, and have systematically varied pH
values in the range of 10-13 within the corresponding, associated hydrothermal reactions.

The XRD results shown in Figure 3 suggest that the pH values have had little if any
impact upon either the chemical composition or the crystal structure of the resulting
nanostructures. Indeed, in these four different samples, all of the peaks can be ascribed to a
single-crystalline willemite structure (JCPDS #37-1485), with no indication of impurities.

On the other hand, the pH values have dramatically affected the observed morphology, as
revealed in Figure 4. Specifically, as the pH was increased from 10 to 13, the shapes of the
resulting materials altered from micron-sized wires (Figure 4A and 4B) to nanoscale wires
(Figure 4C) and finally into nanoscale pillars (Figure 4D). A detailed summary of their
respective sizes is presented in Table 2. Based upon our observations, smaller structures (i.e.
'novel' nanopillars with diameters of ~ 30 nm and lengths of ~ 100 nm) were preferably
produced at higher pH values, whereas larger motifs (i.e. nanowires with diameters of ~ 400 nm
and lengths of ~ 8 μm) predominated at relatively lower pH values. We have therefore
hypothesized that the reaction mechanism is dependent upon the concentration of NaOH.

Indeed, according to a prior report that utilized a similar hydrothermal synthesis approach, during the early stage of the reaction, the Zn precursor first interacted with NaOH solution, thereby forming bulk ZnO, before further combining with and reacting with the SiO_2 precursor to create smaller Zn_2SiO_4 nanostructures.[39] According to this work, at 220°C, ZnO formed within the first hour, followed by its transformation to a $Zn_4Si_2O_7(OH)_2$ (i.e., hemimorphite) intermediate within the next 3 to 6 hours, and finally its ultimate conversion to Zn_2SiO_4 after a period of 10 hours. In fact, the hemimorphite species has been previously shown to serve as an intermediate in analogous hydrothermal syntheses, and can be produced when the temperature is at least 150 to 175°C.[40] Most importantly, the formation of ZnO as a clear intermediate species during the hydrothermal synthesis of Zn_2SiO_4 has been verified by multiple reports.[14, 39, 41]

In effect, it has been shown that the growth rate of ZnO nanostructures depends upon the concentration of the base in solution.[42, 43] Specifically, at high NaOH concentrations, the growth of ZnO nanostructures can be hindered not only by (1) the incidence of negatively charged species[44] such as $Zn(OH)_3^-$ or $Zn(OH)_4^{2-}$ present in the reaction mixture but also by (2) the presence of an effective passivating layer of cations[43] (e.g., Na^+ or K^+) on the external surfaces of the ZnO nanocrystals. Thus, we believe that in our system, the size of the ZnO intermediary species serves as a structural "template" for the additional formation of Zn_2SiO_4 and that the observed dimensions of the silicate product directly depend upon the corresponding amount of NaOH present, accounting for the size limitations and variations observed.

3.3. Optimization of synthetic conditions and reaction mechanism

Our proposed reaction mechanism is shown in Figure 5. Indeed, as a collective summary of the two previous sets of experiments, we have been able to demonstrate that the synthesis process is sensitive to both the pH value as well as to the Mn dopant concentration. In terms of

their relative importance in dictating the dimensions of as-preparing Zn_2SiO_4 nanostructures, our findings suggest that pH plays a primary role, whereas Mn dopant concentration is important but less significant. Specifically, the magnitude of the pH value dictates the upper limit of the overall size observed associated with the resulting products, which could attain dimensions of up to microns at low pH. By contrast, the dopant Mn concentration impacts upon the stability of these micron-scale and nanoscale structures in which a higher Mn dopant level appears to destabilize the formation of larger structures while promoting generation of smaller nanowires and nanorods.

Specifically, these two factors give rise to synergetic effects with respect to the morphology of the resulting materials. For example, large nanowires can be synthesized under either (i) reduced Mn concentrations (including the absence of Mn dopant altogether) and/or (ii) relatively low pH values (up to 10). This scenario is highlighted by the yellow arrows, shown in Figure 5. Conversely, small nanorods can be produced by either (i) increased Mn concentrations (> 4%) and/or (ii) relatively elevated pH values (>10). This pathway is marked with red arrows, illustrated in Figure 5.

As suggested earlier, we hypothesize that the creation of our Zn_2SiO_4 nanowires is associated with the successive formation of intermediates of ZnO and $Zn_4Si_2O_7(OH)_2 \cdot H_2O$. In the pathway designated by the yellow arrows, these species have been reported as possible precursors to Zn_2SiO_4, as per the prior work of Peng *et al.*'s on a similar system.[39] Specifically, it is postulated that during the hydrothermal reaction, a "splitting process" occurs in which over the course of the reaction, the coarser bulk $Zn_4Si_2O_7(OH)_2 \cdot H_2O$ morphologically evolves and 'splits' into relatively smaller and more structurally well-defined Zn_2SiO_4 nanowires and nanorods. This process is accompanied by a corresponding chemical phase transformation from $Zn_4Si_2O_7(OH)_2 \cdot H_2O$ to Zn_2SiO_4. This 'dehydration' of the intermediate oxide is apparently

driven by H_2O molecules, which have likely de-intercalated from within the interlayer spaces of the $Zn_4Si_2O_7(OH)_2 \cdot H_2O$ itself.

Therefore, in order to verify that our system followed a similar reaction mechanism, we have probed not only the crystal structure but also the morphology of the product at a reasonably early time point associated with the hydrothermal reaction. Indeed, as indicated from both the XRD data and TEM images in Figure S2 and S3, respectively, we have been able to isolate $Zn_4Si_2O_7(OH)_2 \cdot H_2O$ nanocrystals, possessing irregular and micron-sized shapes, thereby supporting our hypothesis.

Hence, to achieve Zn_2SiO_4 nanostructures incorporating not only preferred morphologies with reliable and reproducible chemical compositions but also reasonably well-pronounced photoluminescent properties, we have specifically chosen to prepare samples with 3%, 4%, 6%, and 8% Mn dopant levels and have tuned the pH values accordingly for each individual sample. Specifically, the optimized pH values for these four chemical compositions are 12, 12, 11, and 10, respectively. The XRD patterns and TEM images are correspondingly shown in Figure 6 and 7, and are indicative of highly crystalline and monodisperse Zn_2SiO_4 nanowire structures. In addition, larger-scale SEM images of all four Mn-doped Zn_2SiO_4 samples are provided in Figure S4, further corroborating the inherent structural uniformity and homogeneity of these nanowire morphologies. A summary of detailed morphological data has been provided in Table 3, and these results imply that all of these motifs possessed comparable diameters as well as lengths.

In addition, we have collected high-resolution TEM (HRTEM) images as well as corresponding SAED patterns (Figure S5). As highlighted in Figures S5A through S5D, the crystalline planes within the nanowires are perfectly aligned, an observation which is consistent with the single-crystalline nature of as-prepared Zn_2SiO_4 nanowires. Moreover, as for SAED

patterns in Figure S5E through S5H, we have observed a number of bright, scattered dots, a finding plausibly indicative of a superimposition of multiple individual single-crystalline structures.[45, 46] We should note that due to (i) the relatively small dimensions of our samples from a SAED perspective (i.e., nanomaterials measuring ~700 nm in length and ~30 nm diameter) as well as (ii) the aggregated and somewhat clustered nature of our as-prepared wires, it was extremely difficult to obtain a definitive SAED pattern of discrete, individual wires. As such, all of the SAED patterns were acquired from regions that were composed of ~30 to 50 intertwined nanowires, organized like a network. Nevertheless, we believe that these data ruled out the possibilities of our samples being either polycrystalline or amorphous, which would have typically resulted in the formation of diffuse "ring patterns".[46] In summary, the presence of clearly visible lattice fringes within the HRTEM images of individual entities as well as the relatively sharp diffraction spots noted in the acquired SAED patterns (Figure S5) are mutually consistent with the highly crystalline nature of our as-prepared Mn-doped Zn_2SiO_4 nanowires.

As well, to further probe the chemical environment associated with the Mn dopant, XPS analysis was performed on the desirable Zn_2SiO_4: Mn (4%) sample, with the undoped Zn_2SiO_4 system analyzed in parallel as a control sample. Within all of this data analysis, as-collected spectra were calibrated by the C 1*s* signal at the 284.6 eV peak position.[11] A wide ranging survey spectrum (Figure S6) was recorded, which confirmed that no extraneous elements were present. Upon comparing the sample incorporating a 4% Mn dopant with that of the undoped sample, a tiny Mn *2p* peak was detected, associated with a binding energy of around 640 eV. The Mn $2p_{3/2}$ spectra, as highlighted in Figure S7, reveals that the position of the Mn $2p_{3/2}$ peak is located at 641.5 eV and can be ascribed to a Mn^{2+} species.[47, 48]

We also further explored the relative positions and amounts of both Zn and Mn. Figure S8 illustrates the relevant spectra, associated with the Zn $2p_{1/2}$ and Zn $2p_{3/2}$ orbitals. A slight positive shift towards higher energies can be observed for all of the peaks associated with the Zn_2SiO_4: Mn (4%) sample as compared with their undoped counterparts. One explanation for this apparent shift upon doping is that (i) the ionic radius (0.80 Å) of Mn^{2+} is relatively larger than that of Zn^{2+} (0.74 Å) and that (ii) the substitution of Zn^{2+} with Mn^{2+} within the underlying lattice could result in an observed increased binding energy of Zn itself.[49] Hence, the distinctive energy signature of the doped silicates is consistent with the idea of Mn ions partially replacing the corresponding Zn within the lattice.

In our subsequent optical studies of CdSe QD - Zn_2SiO_4 heterostructures, we have focused on thin nanowires due to their better size monodispersity as compared with their nanowire counterparts. Furthermore, the aspect ratio of these nanowires is sufficiently high enough (at least 20: 1) to take advantage of the favorable attributes of one-dimensional motifs. Specifically, anisotropic materials tend to possess extended facets, a lower amount of surface defect sites, as well as a continuous and direct pathway for photo-generated electrons and holes to travel, as previously discussed.

3.4. Optical Properties of as-prepared Mn-doped Zn_2SiO_4 nanowires.

The photoluminescent properties of our series of Zn_2SiO_4 nanocrystals have been studied, as shown in Figure 8. Essentially, most of the samples exhibit luminescence at a peak wavelength of 523 nm upon a UV excitation of 265 nm. Our results correlate perfectly well with most of the relevant literature, that have suggested the presence of a 'green' emission band at around 525 nm under similar excitation conditions.[5, 50, 51] As we have determined the oxidation state of Mn within our samples to be +2 through XPS analysis, this emission behavior can likely

be assigned to a $^4T_1$ to $^6A_1$ transition of Mn^{2+}, as opposed to either potentially equally plausible ^2E to $^4A_2$ or $^2T_1$ to $^4A_2$ transitions which are associated with Mn^{4+} ions.[52] Specifically, within the Zn_2SiO_4 host, the Mn^{2+} ion is substitutionally incorporated within a Zn^{2+} lattice site possessing a tetrahedral site symmetry, thereby forming a Mn_{zn}^{2+} luminescent center.[53] The energetically excited $3d$ electrons associated with the Mn_{zn}^{2+} ion relax radiatively from the $^4T_1$ excited state to the $^6A_1$ ground state, thereby leading to the observed green PL emission.

As an important note, we have observed that most of our nanowire samples have yielded measured peak intensities of approximately 10^6 photon counts. In the recent literature, it has been relatively rare for groups to report on absolute PL intensities. In fact, much of the work in the past few decades has focused on exploring parameters which affect the *relative* PL output of their samples, and as such, these studies tend to provide PL data in terms of arbitrary units (a.u.). Notwithstanding this tendency, we were indeed able to find PL intensity data reported on several nano-sized Mn-doped Zn_2SiO_4 samples, characterized by dimensions ranging from tens of nanometers to hundreds of nanometers. These results were also within the range of $1x10^5$ to $1x10^6$ photon counts.[54-56] Our findings herein are quite comparable, thereby proving that our PL intensity values are within a reasonable and acceptable range.

In terms of notable trends, we have indeed observed a volcano-shaped relationship between the dopant concentration of Mn and the resulting photoluminescent intensities, peaking at 4%. Many reports have observed a similar trend within a series of Mn-doped Zn_2SiO_4 samples.[5, 9, 57] To explain this observation, it has been demonstrated that an increase in the doping level may lead to the formation of Mn^{2+} ion pair centers that may substitute for Zn^{2+} at spatially adjacent, nearest neighbor Zn^{2+} sites.[32, 58] Meanwhile, the elevated dopant level may also result in the formation of closely-spaced dopant ions that preferably form Mn-O-Mn

structures, which are known to exhibit little to no luminescence; this behavior is exemplified by manganese oxide.[58] Moreover, exchange interactions between Mn^{2+} ion pair centers created under these higher dopant conditions may allow for excess excitation energy to potentially dissipate through alternative electronically 'non-radiative' transitions, which may reduce the magnitude of the observed emission efficiency.[59, 60] This so-called "quenching concentration effect" has been previously reported for a variety of doping hosts.[61] Therefore, herein, to ensure not only optical reliability and interpretability but also maximum signal-to-noise ratios, we will be focusing on samples consisting of 4% Mn-doped Zn_2SiO_4 nanowires and their corresponding heterostructures, as these are considered to be 'optically optimized'.

3.5. Probing the optical properties of CdSe QD - Mn: Zn_2SiO_4 heterostructures

In order to ensure the formation of a chemical bond and an electronically viable connection between CdSe QDs and Mn-doped Zn_2SiO_4 nanowire structures, we have fabricated CdSe QD - Mn: Zn_2SiO_4 heterostructures using mercaptopropionic acid (MPA) as the linker molecule. A representative TEM image coupled with the corresponding magnified image of the interfacial region between the QDs and the underlying metal oxides associated with these CdSe QD – Mn: Zn_2SiO_4 heterostructures, possessing a Mn dopant level of 4%, are highlighted in Figure 9A and 9B, respectively.

It is apparent that the CdSe QDs experienced a certain level of aggregation and agglomeration, similar to observations we have made with our previous analogous QD-based heterostructured systems.[21, 26, 31] Nonetheless, the spatial distribution of the quantum dots is still relatively homogeneous with respect to the Zn_2SiO_4 nanowires beneath. In addition, the corresponding EDS elemental mapping spectra, shown in Figure S9, suggest a rather effective overlap between the Cd and Se signals associated with CdSe QDs and the Zn, Si, O, and Mn

signals characteristic of Mn: Zn_2SiO_4 nanowires. As such, both the electron microscopy data as well as the EDS results are consistent with the successful attachment of CdSe QDs onto the outer surfaces of the Mn: Zn_2SiO_4 nanowires.

The optical properties of these as-prepared heterostructures including control samples have also been examined. First, optical characterization data for as-prepared CdSe QDs are included in Figure S10. These results suggest that the QDs possess a narrow and monodisperse size distribution, centered at 4.8 nm.

In terms of the corresponding heterostructures, the PL spectra of MPA-capped CdSe QDs, 4% Mn: Zn_2SiO_4, as well as the as-prepared heterostructures comprising these two constituent component species have been collected and are depicted in Figure 10. Specifically, under an excitation wavelength of 265 nm, the emission band at 523 nm, associated with Mn^{2+} in Zn_2SiO_4, exhibited a significant quenching effect after quantum dot attachment.

A number of explanations are possible to account for this phenomenon. For example, we can attribute this observation to a plausible energy transfer from Mn^{2+} to the CdSe QDs, since the emission energy of 2.37 eV (equivalent to a wavelength of 523 nm) is comparable to that of the bandgap of the CdSe QDs herein (i.e. 2.05 eV). Similar behavior has also been observed with analogous CdSe QD - $LaPO_4$: RE heterostructures, previously studied.[25] Alternatively, this observation could also originate from a re-absorption of radiation emitted by Mn^{2+} dopant ions by the adjoining CdSe QDs. This is a common scenario for heterogeneous systems incorporating light sensitizers such as quantum dots.[62] Typically, energy transfer relies on a degree of coupling between the donor and the acceptor wherein the strength of coupling decreases with increasing donor-acceptor distance.[63, 64] A study conducted by Federspiel *et al.* has shown that the energy transfer rate is largely reduced when this distance exceeds 10 nm.[65] In our specific case, CdSe

QDs were immobilized onto the external surfaces of nanowires. Thus, it would be reasonable to expect that Mn^{2+} dopant ions localized near the surface would have an opportunity to interact the most with adjacent CdSe QDs. However, farther away from the surface, any such interactions between these two species will be likely diminished due to the aforementioned distance-dependence and electrostatic screening induced by the presence of the underlying inorganic oxide matrix. Hence, a combination of energy transfer and re-absorption can potentially explain the observed enhancement of the CdSe QD signal, whereas energy transfer is likely to be solely responsible for the diminution of the Mn^{2+} band intensity.

Nonetheless, we should note that the enhancement of the CdSe QD signal within the heterostructure obtained at an excitation of 265 nm is rather small in terms of magnitude. At the same time, we have also observed a nearly complete quenching of the Mn emission signal. Based upon our own experience in analogous systems as well as upon observations made in the prior literature, we find that energy transfer usually results in a relatively small net degree of total energy loss.[25, 66] In other words, the amount of enhancement associated with the plausible energy transfer from the band emission of CdSe QDs should essentially be the same magnitude as and ought to balance out the quantity of energy decrease associated with the $^4T_1$ to $^6A_1$ transition of Mn within Mn-doped Zn_2SiO_4.

This hypothesis does not necessarily explain our observations herein as what we have found is evidently different. Therefore, it is reasonable to conclude that our heterostructures may have experienced an overall and dramatic loss in terms of the observed photoluminescent signal profile. We attribute this observation to a plausible charge transfer occurring from the CdSe QDs to the Mn dopant, a phenomenon which has been previously reported in similar types of systems.[67, 68] This process will be explained in more detail in the following section. Nevertheless,

we should note that the plausible existence of both energy transfer and charge transfer within a single discrete system, when excited using a monochromatic beam, has rarely been reported, and therefore, this observation represents one of the major and unexpected findings within this work.

We have prepared an energy diagram based upon literature values[53, 69] of the positions of the conduction band (CB) and the valence band (VB) of Zn_2SiO_4, as well as of the HOMO and LUMO positions associated with CdSe, the Mn dopant, and the MPA ligand, as shown in Figure 11. Specifically, the LUMO of CdSe is located at a higher potential than that of the $^4T_1$ state of Mn^{2+} within the Zn_2SiO_4 lattice, denoting a favorable scenario for electron transfer. Similarly, the HOMO of the MPA ligand is located at a higher potential than that of CdSe, thereby promoting a compensatory hole transfer from CdSe to MPA. That is, the preferred 'migratory' routes of both electrons and holes are in opposite directions to each other. However, the HOMO of CdSe is located at a higher potential than that of the $^6A_1$ state of Mn^{2+}, which hinders possible hole transfer from CdSe to Mn^{2+}. As a result, the PL signal of the CdSe QDs will decrease dramatically because of the existence of charge transfer occurring to the metal dopant, thereby plausibly leading to a PL quenching effect. Nevertheless, the PL signal of CdSe QDs exhibited a small net increase, likely owing to competing energy transfer and charge transfer processes.

On the other hand, upon excitation at 388 nm, the CdSe QDs exhibited a significant PL quenching effect within the CdSe QD - 4% Mn: Zn_2SiO_4 heterostructures as compared with the MPA-capped CdSe QDs by themselves. Indeed, as shown in the energy diagram in Figure 11, the excitation energy (i.e. equivalent to a photon energy of 3.2 eV) is insufficient to excite the Mn^{2+} dopant species within our doped Zn_2SiO_4 samples. Therefore, only the CdSe QDs are photoexcited and give rise to a band emission at 614 nm. Moreover, by analogy with circumstances discussed previously, the as-generated photo-electrons will preferably transfer

towards Mn^{2+}, whereas the analogous photo-generated holes will likely transfer towards the MPA ligands. This effective and plausible charge transfer process likely accounts for the corresponding quenching effects observed within the overall PL spectra of the CdSe QD - Mn: Zn_2SiO_4 heterostructures in particular.

Nevertheless, we recognize that the degree of QD aggregation might also have possibly accounted for the observed quenching in the PL spectra. To address this point, we have added in TEM images (Figure S11) of MPA-capped CdSe QDs, both before and after attachment to Mn: Zn_2SiO_4, to highlight and demonstrate that the degree of QD aggregation and QD dispersion had not been either noticeably or adversely affected by the process of forming the desired QD-metal oxide heterostructures. Additionally, a control experiment has been conducted wherein CdSe QDs have been attached onto undoped Zn_2SiO_4 nanowires, and the corresponding PL data have been recorded, as shown in Figure S12. Indeed, the PL intensity of CdSe QDs exhibited little if any decrease after immobilization onto undoped Zn_2SiO_4 nanowires, thereby implying that the Mn^{2+} dopant is the primary cause of the observed signal quenching. In other words, based upon both of these two observations, changes in the optical properties of QDs within both free MPA-capped CdSe QDs and MPA-capped CdSe QD - Mn: Zn_2SiO_4 heterostructures cannot be reasonably ascribed to either packing or aggregation considerations.

Furthermore, the lifetimes of CdSe QDs incorporated within these heterostructures were acquired and compared with respect to that of their free and bare analogues (i.e., CdSe QDs alone) at different excitation wavelengths. These data are summarized in Tables S1. We find that, upon formation of the heterostructures, the lifetimes of CdSe QD species have perceptibly diminished. These observations can be reasonably attributed to the reduction in the PL output of the immobilized CdSe QDs when excited at 388 nm, thereby further confirming and verifying

that energy transfer and charge transfer both likely occur and are significant within these composite hierarchical systems.

Collectively, the series of spectra acquired at excitation wavelengths of both 265 nm and 388 nm have confirmed the close optoelectronic interactions and interplay between the constituent CdSe QDs and the adjoining Mn: Zn_2SiO_4 within our heterostructures. Specifically, when both materials have been photoexcited, energy transfer likely occurs from Mn^{2+} to CdSe QDs, whereas charge transfer reasonably takes place from the CdSe QDs to the Mn^{2+} species. When CdSe QDs are photo-excited alone, only charge transfer is relevant to consider. Indeed, according to our proposed mechanism, when both materials are excited, the energy absorbed by Mn: Zn_2SiO_4 can be transferred to CdSe QDs through a plausible energy transfer process, and subsequently utilized to generate photo-electrons. Hence, we believe that our heterostructures denote viable architectures for photovoltaic cell configurations, because the wavelength range of potentially usable incident radiation within these composites is likely to be significantly broader upon incorporation of Mn: Zn_2SiO_4 possessing a larger bandgap (i.e. 5.5 eV).

In a separate experiment, we have also collected the UV-visible spectra of our as-synthesized Mn-doped Zn_2SiO_4 nanowires, of MPA-capped CdSe QDs, as well as of the resulting QD-metal oxide heterostructures, as shown in Figure S13. The results indicate not only that the Mn-doped Zn_2SiO_4 possessed a broad absorption range within the entire solar spectrum region of ~ 400-700 nm but also that the as-prepared heterostructures combine the absorption potential of both of the individual constituent components, thereby mitigating for the relatively lower light-absorbing capability of CdSe QDs alone, beyond 600 nm.

4. Conclusions

In this work, we have synthesized Mn-doped Zn_2SiO_4 nanowires through a facile hydrothermal approach. The effects of reaction parameters and variables, including pH and Mn dopant levels, upon the as-prepared crystal structure as well as the morphologies of the resulting materials formed, have been systematically probed. We have especially highlighted the use of dopant ion concentration as a fundamentally generalizable, tunable, and tailorable synthetic knob in order to substantively affect the resulting observed morphology, i.e. both size and shape, and consequently, the corresponding optical properties detected of a targeted nanomaterial. Indeed, very few reports have emphasized the key role of dopant in determining morphology, especially with respect to solution-phase-based protocols.

We find that the pH value and the Mn dopant level yielded contradictory behavioral trends towards the overall sizes of the resulting one-dimensional nanostructures produced. Specifically, micron-sized wires (with average diameters of ~ 400 nm and lengths of ~ 8 μm) could be synthesized with either reduced Mn concentrations and/or elevated pH values. By contrast, smaller and relatively lesser-reported nanopillars, possessing decreased aspect ratios with average diameters of ~ 30 nm and lengths of ~ 100 nm, could be generated using either increased Mn concentrations and/or lowered pH values. Moreover, we have carefully optimized synthesis conditions to generate a reproducible series of highly crystalline Mn-doped Zn_2SiO_4 1D motifs with well-defined Mn dopant concentrations ranging from 3% to 8%, characterized by a monodisperse size distribution (i.e. average diameters of ~ 30 nm and lengths of ~ 700 nm).

Optically, all of these optimized nanowires were found to exhibit a PL emission peak centered at 523 nm upon an excitation of 265 nm. In addition, the PL signal possessed a volcano-shaped relationship with respect to the Mn dopant level, peaking at 4%. Furthermore, the optical properties of CdSe QD - Mn: Zn_2SiO_4 heterostructures have been analyzed. Our results (Figure

11) have demonstrated a unique and complex system involving both simultaneous energy transfer and charge transfer phenomena between the two constituent components. Specifically, when both materials have been photo-excited, energy transfer likely occurs from the dopant Mn^{2+} species to CdSe QDs, whereas electron transfer tends to materialize from the CdSe QDs to the dopant Mn^{2+} ions. Upon excitation of the CdSe QDs alone, probable charge transfer was found to appear from the CdSe QDs to the adjoining Mn^{2+}. Therefore, we believe that our as-processed heterostructures represent potentially promising motifs as novel light-harvesting materials for QDSSCs, since these composites maintain an essentially broadened light absorption capability, due to their incorporation of a wide-bandgap, dopant-tunable Zn_2SiO_4 material.
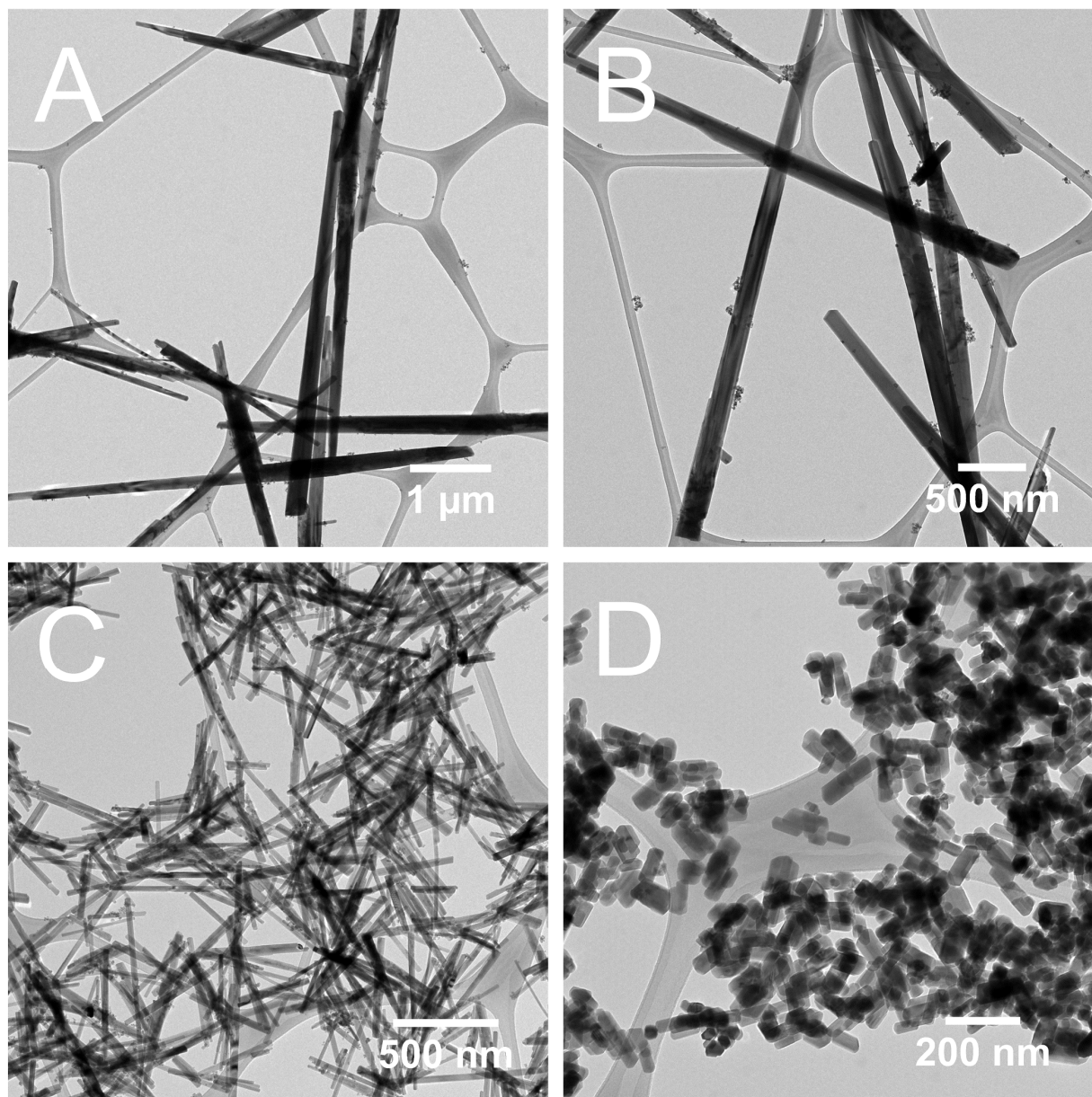
5. Acknowledgements
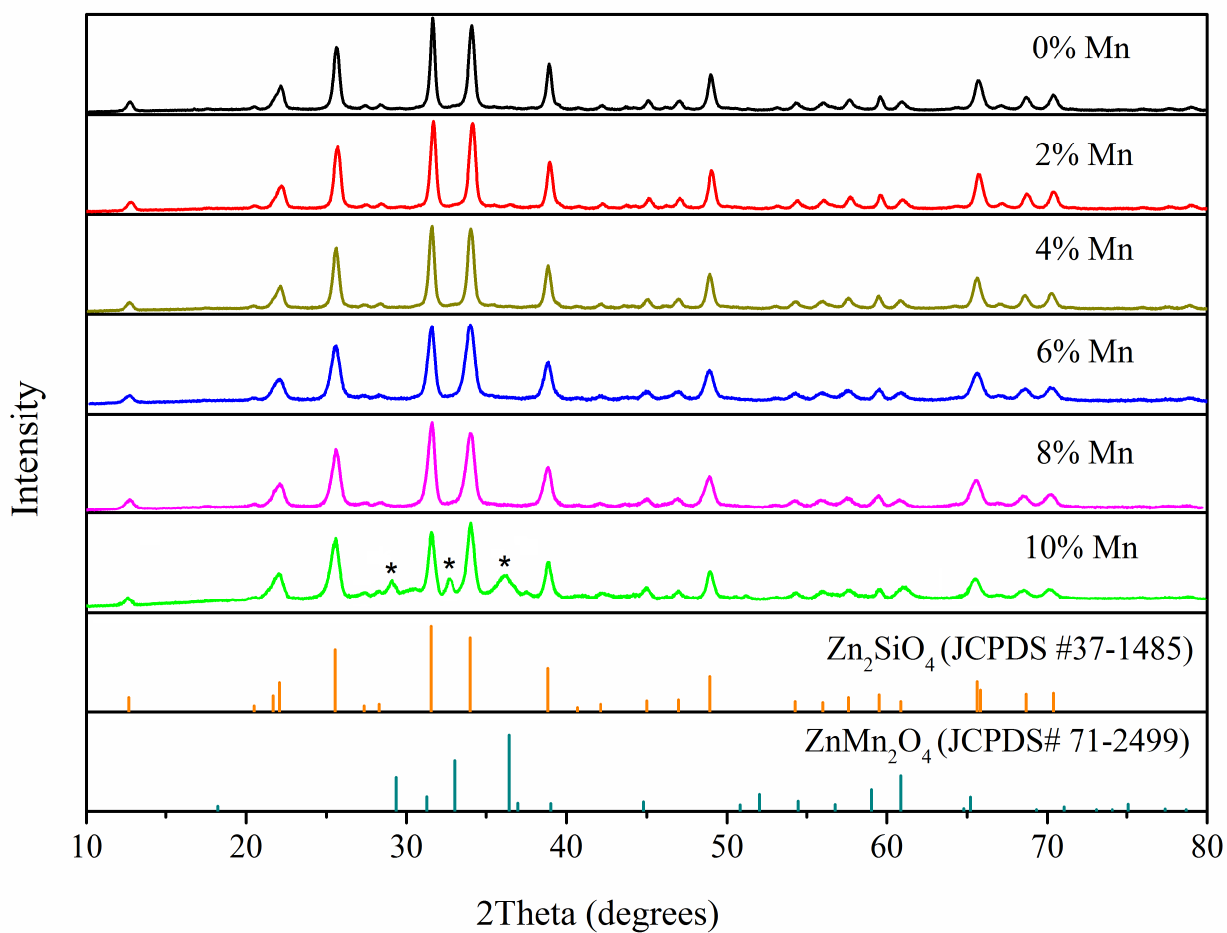
Figure 1. Experimental XRD patterns of a series of as-synthesized Mn-doped Zn_2SiO_4 samples with intended Mn molar dopant concentrations, varying from 0% to 10%. The impurity peaks are labeled with "*". Database standards are shown at the bottom as JCPDS #37-1485 and 71-2499, respectively, for Zn_2SiO_4 and $ZnMn_2O_4$.
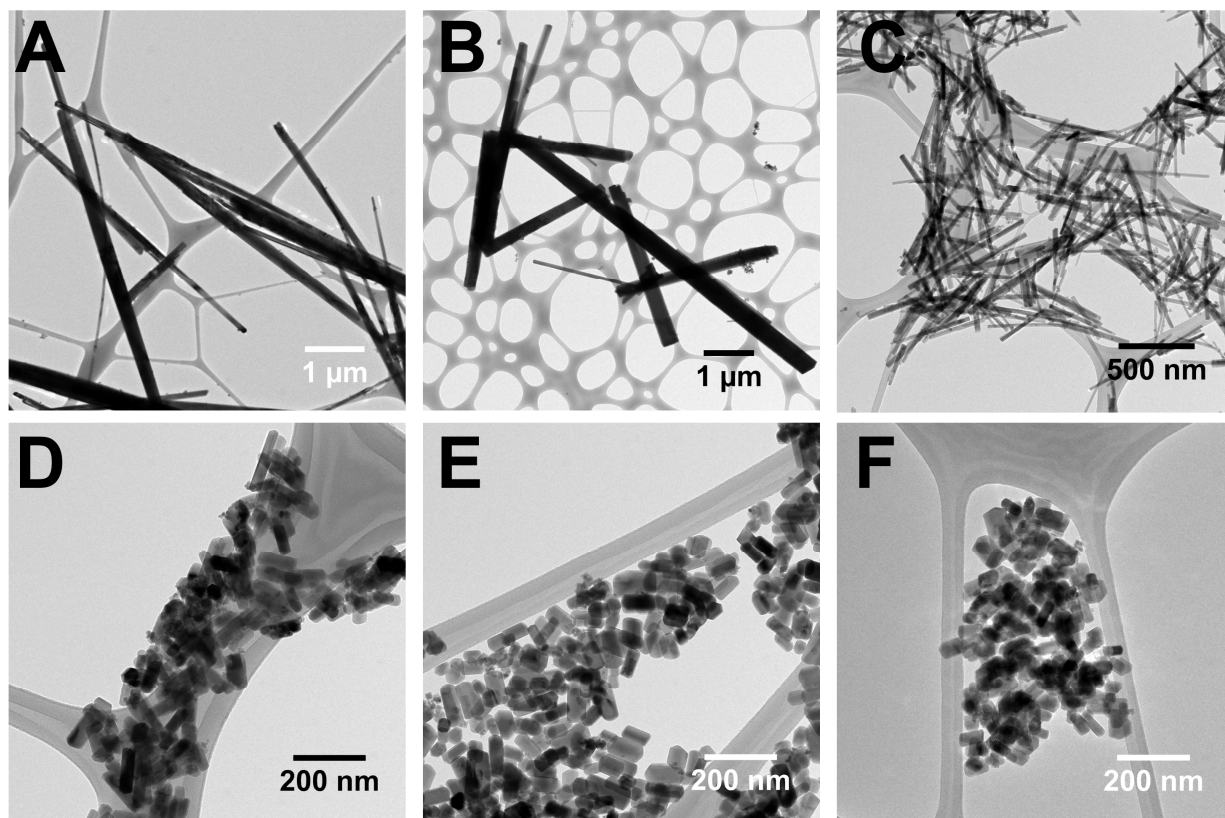
Figure 2. TEM images of a series of as-synthesized Mn-doped Zn_2SiO_4 with intended Mn molar dopant concentrations of (A) 0%, (B) 2%, (C) 4%, (D) 6%, (E) 8%, and (F) 10%, respectively.
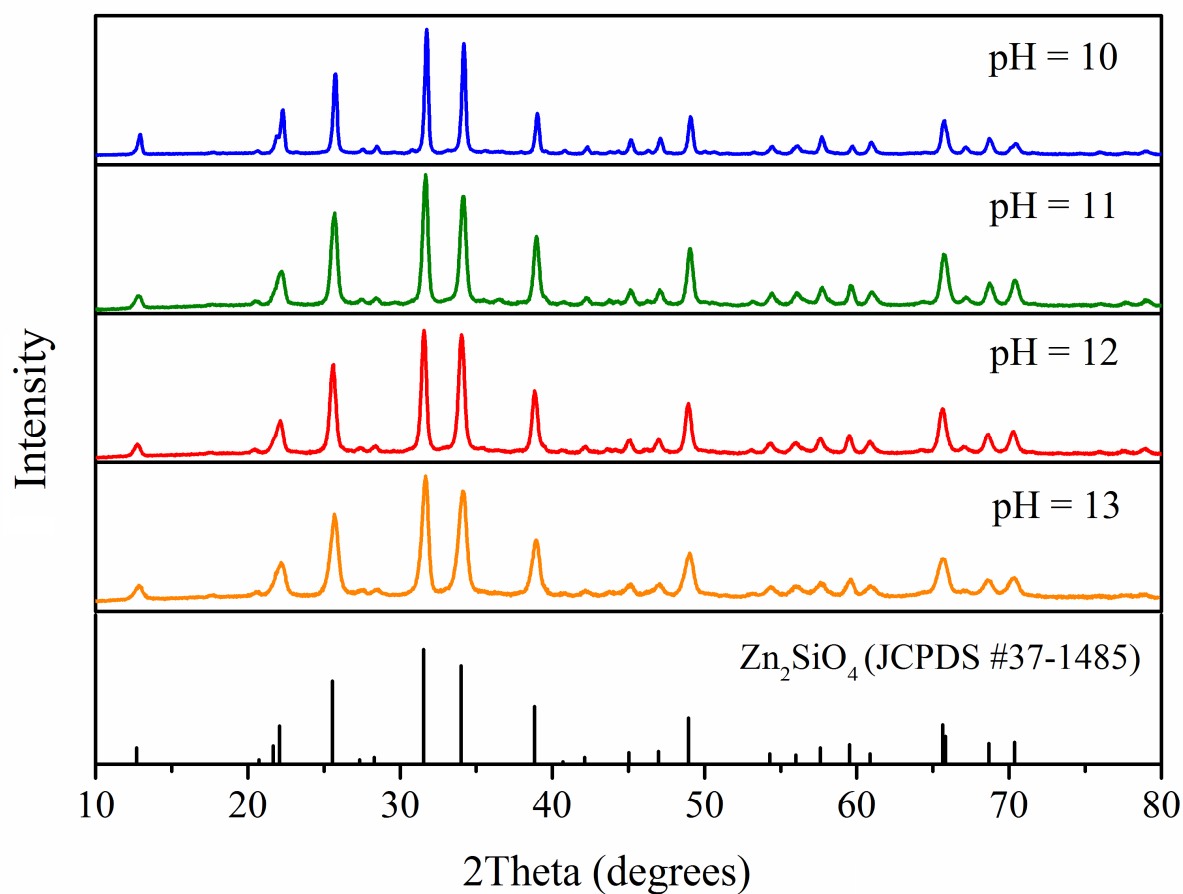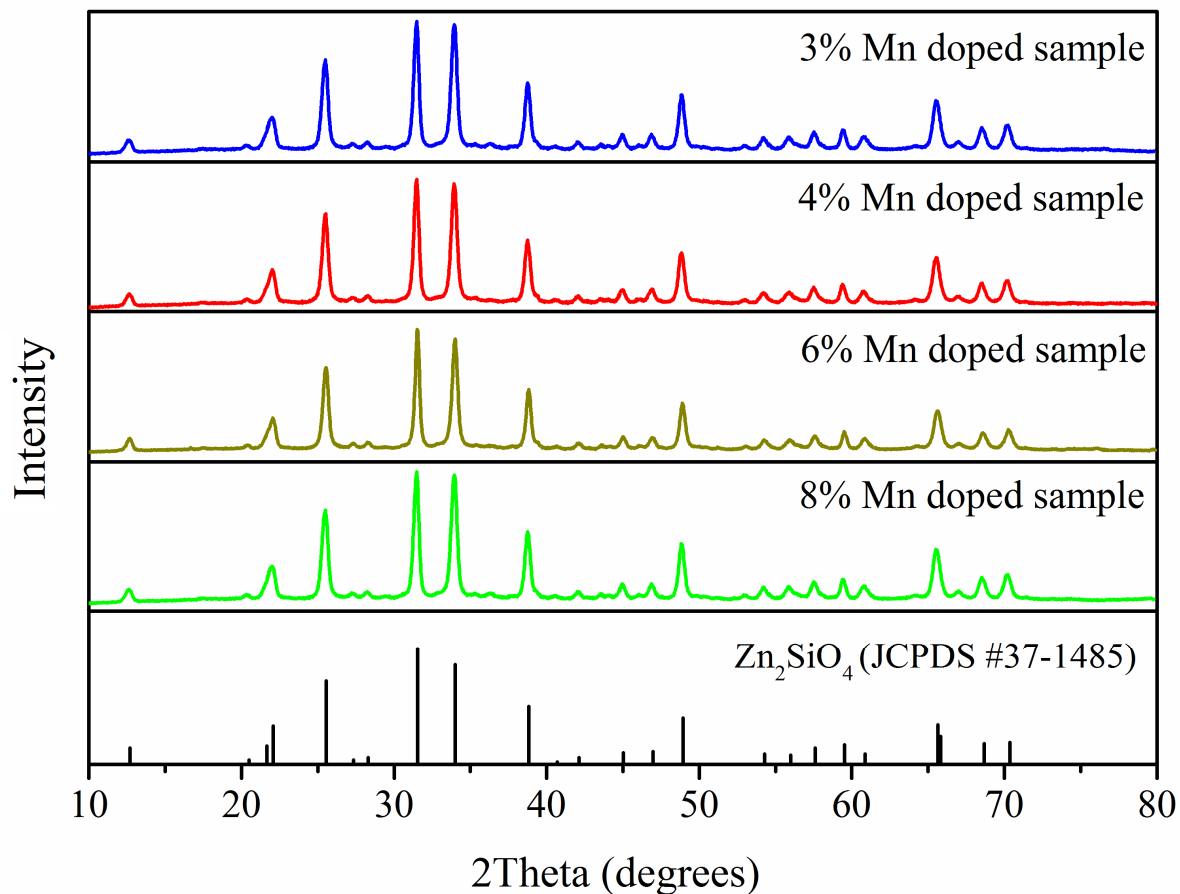
Figure 3. Experimental XRD patterns of a series of as-synthesized 4% Mn-doped Zn_2SiO_4 created under pH values of 10, 11, 12, and 13, respectively. The database standard for Zn_2SiO_4 is shown at the bottom in black.

Figure 4. TEM images of a series of as-synthesized 4% Mn doped Zn_2SiO_4 samples, prepared under pH values of (A) 10, (B) 11, (C) 12, and (D) 13, respectively.
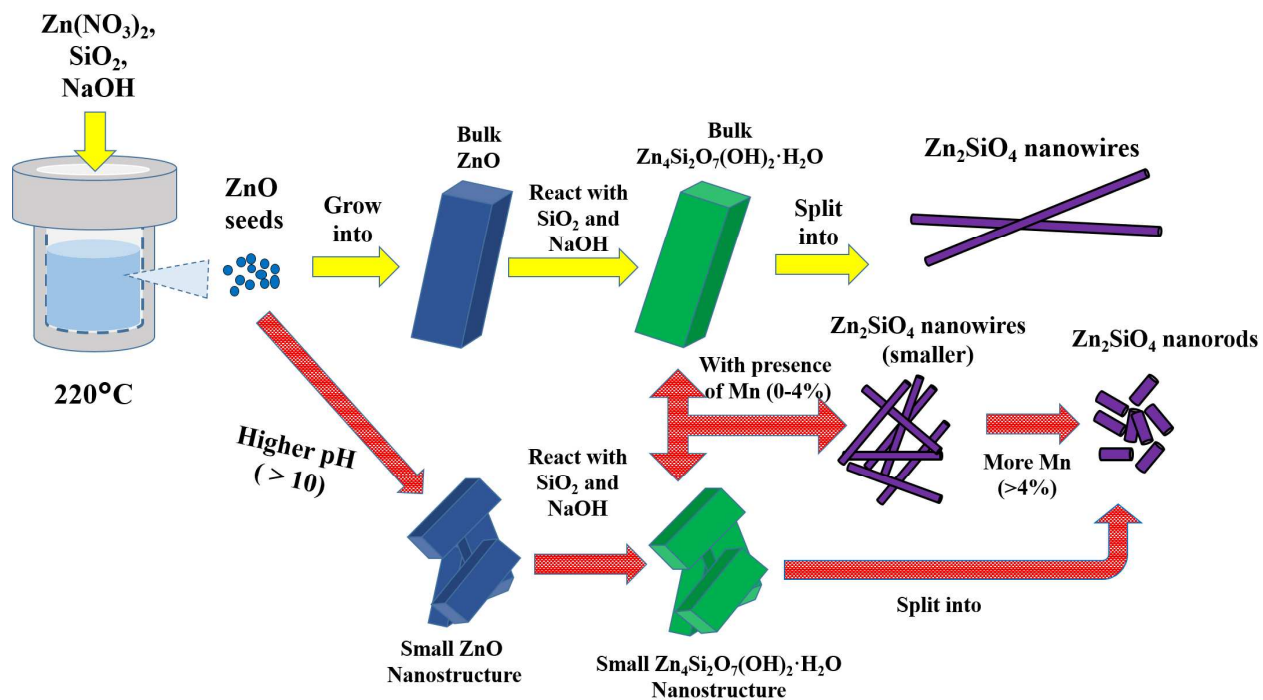
Figure 5. Schematic of the proposed evolution of morphologies as a function of elevated pH values and the presence of Mn dopant species.

**Figure 6.** Experimental XRD patterns of the optimized Mn-doped Zn_2SiO_4 series with intended Mn dopant concentrations of 3%, 4%, 6%, and 8%, respectively. The database standard for Zn_2SiO_4 is shown at the bottom in black.
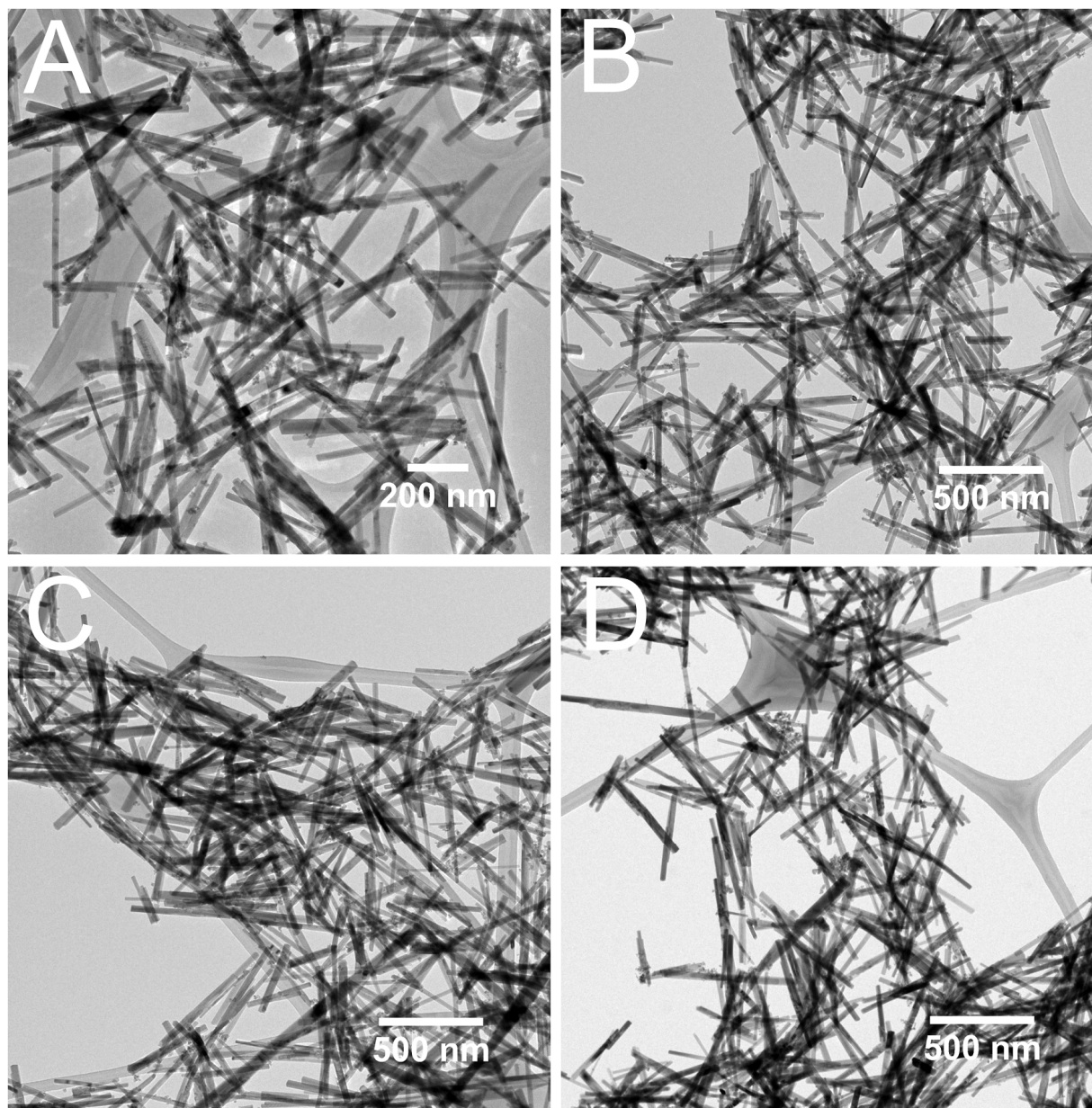
Figure 7. TEM images of an optimized Mn-doped Zn_2SiO_4 series of samples with intended Mn dopant concentrations of (A) 3%, (B) 4%, (C) 6%, and (D) 8%, respectively.
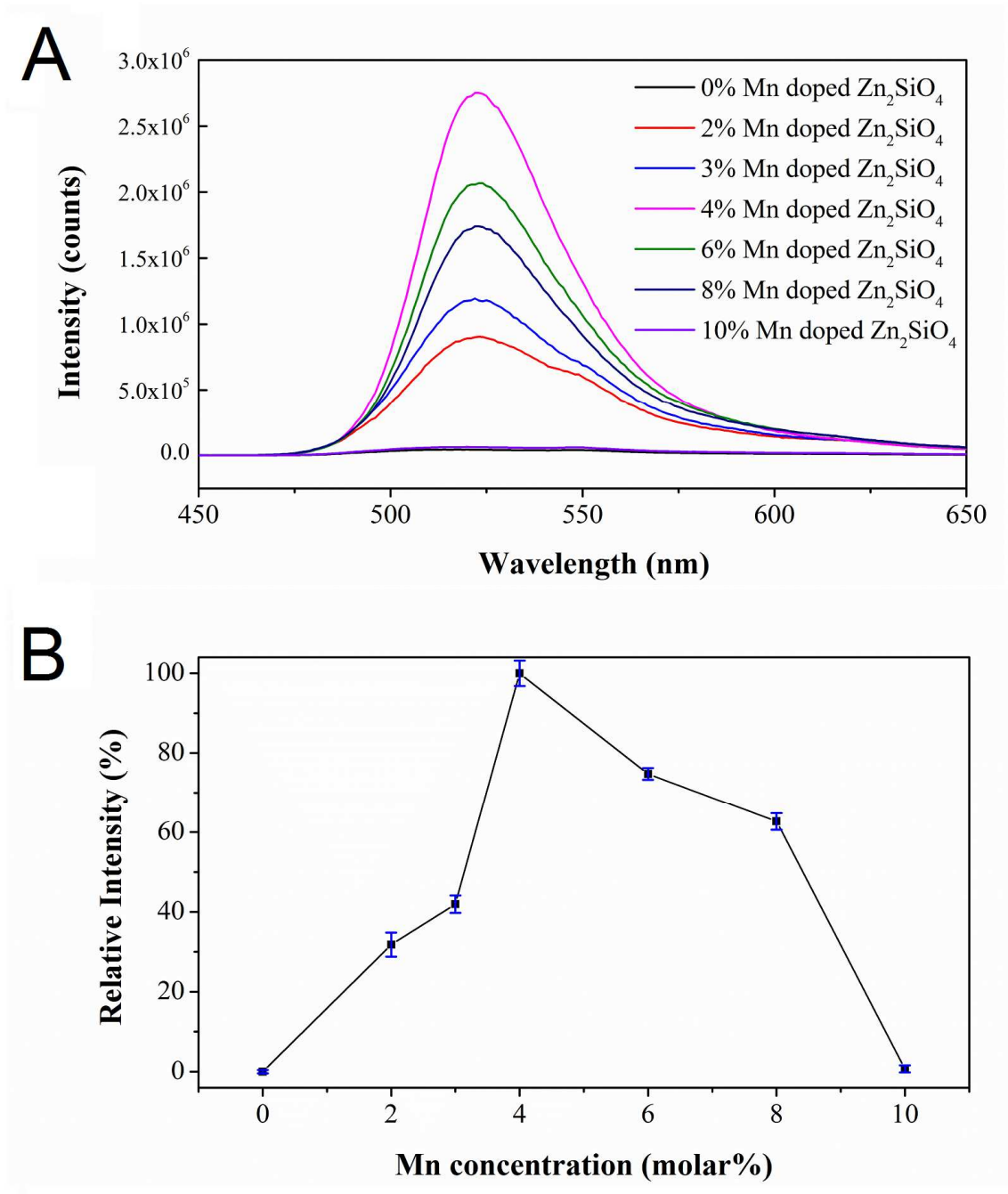
Figure 8. (A) PL spectra of Mn-doped Zn_2SiO_4 samples with various intended Mn dopant ion levels (from 0 to 10%). (B) Relative PL peak intensities (with error bars included) plotted as a function of the intended Mn dopant ion concentration, based upon data presented in panel A.
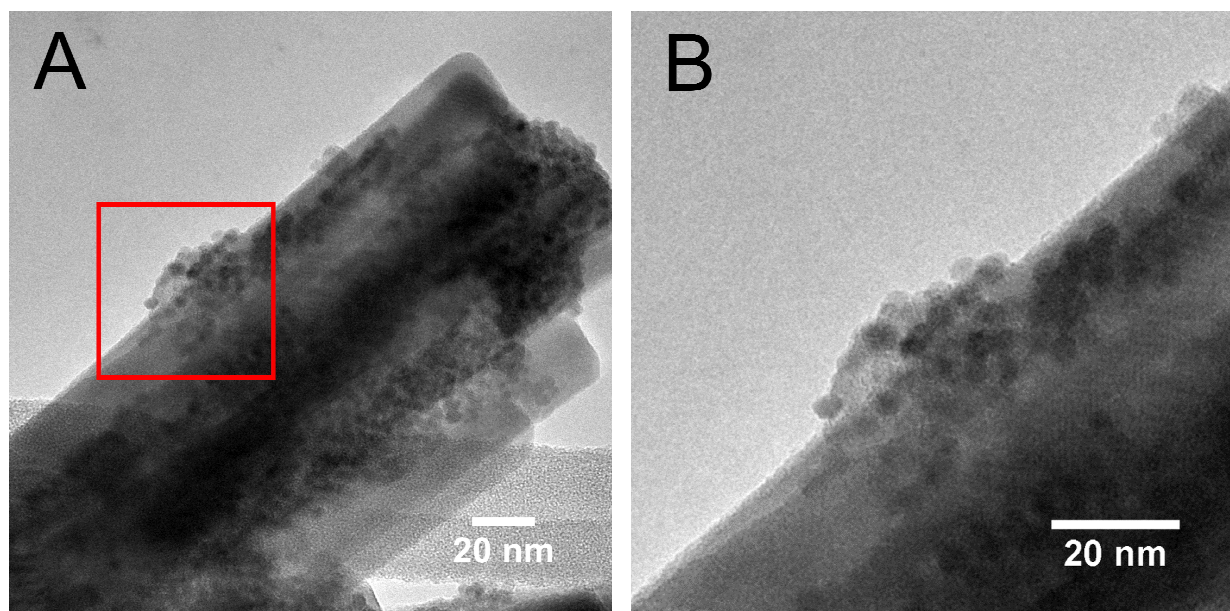
Figure 9. (A) TEM image of CdSe QD - Mn: Zn_2SiO_4 0D-1D heterostructures. (B) A higher magnification image of the interface between the two constituent components of the as-prepared heterostructures.
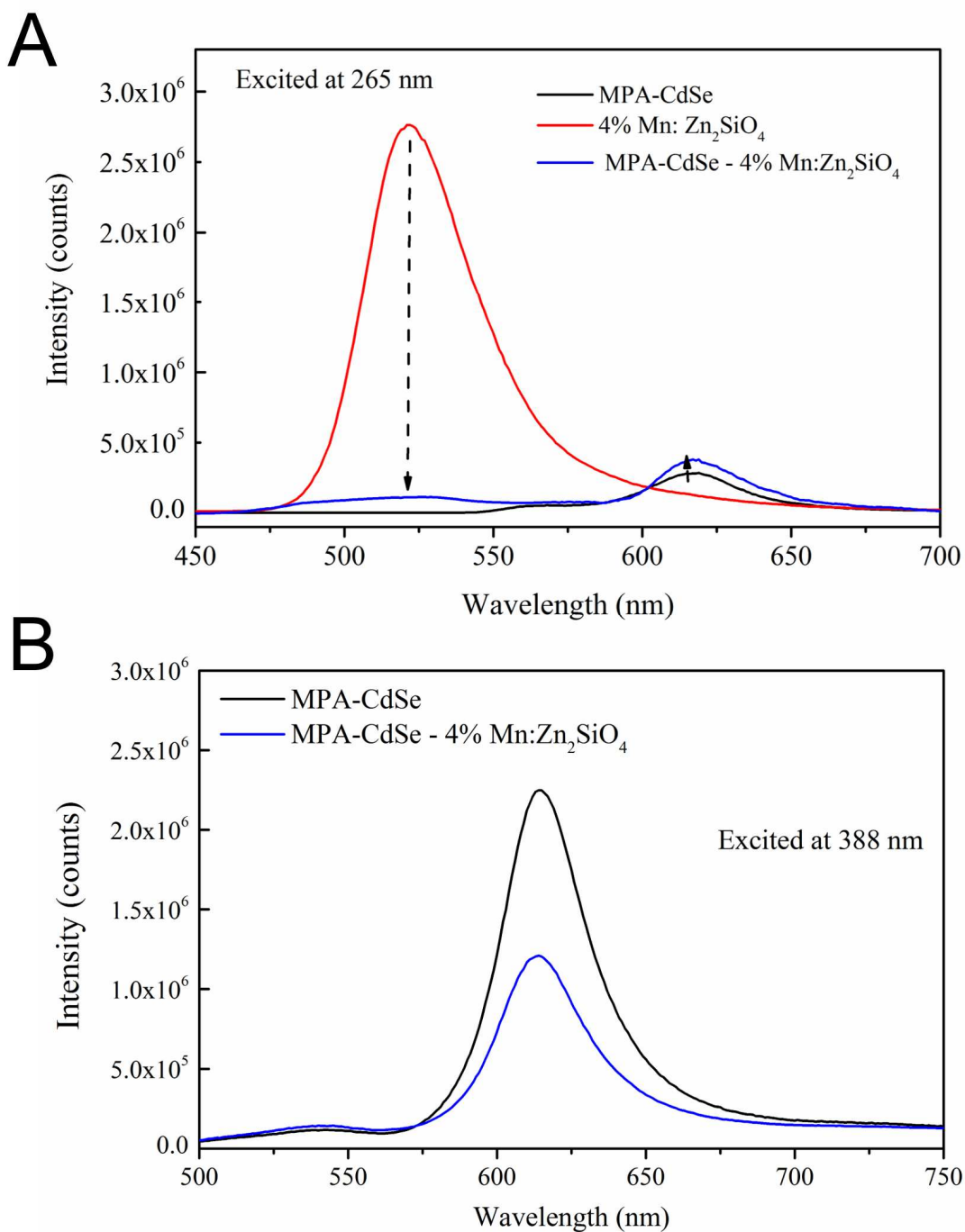
Figure 10. PL emission spectra of MPA-capped CdSe QDs (black), 4% Mn doped Zn_2SiO_4 nanowires (red), as well as MPA-capped CdSe QD - Mn: Zn_2SiO_4 heterostructures (blue), respectively, upon (A) 265 nm and (B) 388 nm excitation, respectively.
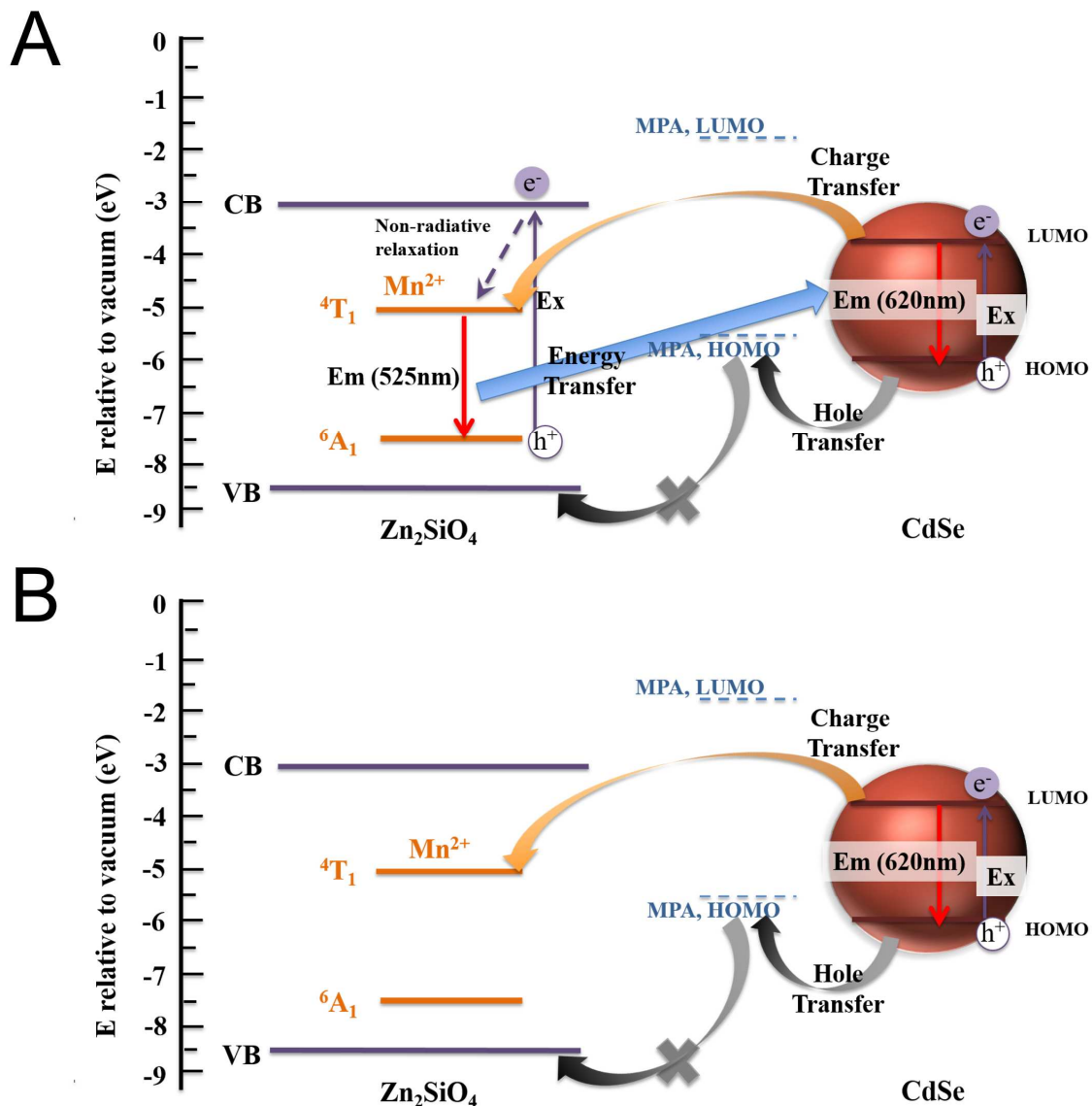
Figure 11. Proposed electronic energy diagram, highlighting the energy band alignments associated with CdSe QDs anchored onto Mn-doped Zn_2SiO_4 nanowires. Potential energy transfer and charge transfer phenomena likely occurring within the heterostructures have been noted upon excitation at (A) 265 nm and (B) 388 nm, respectively. e^- = electron; h^+ = hole; CB = conduction band; VB = valence band; LUMO = lowest unoccupied molecular orbital; and HOMO = highest occupied molecular orbital.

Sample	Morphology and Crystallinity	Dimensions
Pure Zn_2SiO_4	Nanowires, single-crystalline	Diameter of 326 ± 71 nm, length of 8.6 ± 1.5 μm
2% Mn-doped Zn_2SiO_4	Nanowires, single-crystalline	Diameter of 343 ± 91 nm, length of 7.3 ± 1.7 μm
4% Mn-doped Zn_2SiO_4	Nanowires, single-crystalline	Diameter of 29 ± 5 nm, length of 627 ± 82 nm
6% Mn-doped Zn_2SiO_4	Nanopillars, single-crystalline	Diameter of 36 ± 5 nm, length of 119 ± 19 nm
8% Mn-doped Zn_2SiO_4	Nanopillars, single-crystalline	Diameter of 38 ± 6 nm, length of 76 ± 14 nm
10% Mn-doped Zn_2SiO_4	Nanopillars, single-crystalline	Diameter of 34 ± 4 nm, length of 63 ± 8 nm

Table 1. A summary of as-synthesized Mn-doped Zn_2SiO_4 samples possessing different intended

Mn dopant concentrations, in terms of morphology, crystallinity, and spatial dimensions.

Sample	Morphology and Crystallinity	Dimensions
4% Mn doped Zn$_2$SiO$_4$, pH = 10	Nanowires, single-crystalline	Diameter of 413 ± 35 nm, length of 6.4 ± 1.9 μm
4% Mn doped Zn$_2$SiO$_4$, pH = 11	Nanowires, single-crystalline	Diameter of 399 ± 85 nm, length of 7.1 ± 2.2 μm
4% Mn doped Zn$_2$SiO$_4$, pH = 12	Nanowires, single-crystalline	Diameter of 29 ± 5 nm, length of 627 ± 82 nm
4% Mn doped Zn$_2$SiO$_4$, pH = 13	Nanopillars, single-crystalline	Diameter of 31 ± 4 nm, length of 88 ± 23 nm

Table 2. Summary of as-prepared 4% Mn-doped Zn$_2$SiO$_4$ samples, generated under different synthetic conditions associated with varying pH values, ranging from 10 to 13, in terms of morphology, crystallinity, and spatial dimensions.

Sample	Optimized pH value during synthesis	Morphology and Crystallinity	Dimensions
Optimized 3% Mn-doped Zn_2SiO_4	12	Nanowires, single-crystalline	Diameter of 28 ± 7 nm, length of 708 ± 77 nm
Optimized 4% Mn-doped Zn_2SiO_4	12	Nanowires, single-crystalline	Diameter of 29 ± 5 nm, length of 627 ± 82 nm
Optimized 6% Mn-doped Zn_2SiO_4	11	Nanowires, single-crystalline	Diameter of 39 ± 10 nm, length of 695 ± 53 nm
Optimized 8% Mn-doped Zn_2SiO_4	10	Nanowires, single-crystalline	Diameter of 34 ± 6 nm, length of 588 ± 103 nm

Table 3. Summary of Mn-doped Zn_2SiO_4 samples with various intended Mn dopant levels, ranging from 3% to 8%, in terms of their respective optimized synthetic conditions with respect to pH. Data on their morphology, crystallinity, and spatial dimensions are presented.

44

References

1. C. Feldmann, T. Justel, C. R. Ronda and P. J. Schmidt, *Adv. Funct. Mater.*, 2003, **13**, 511-516.
2. T. S. Ahmadi, M. Haase and H. Weller, *Mater. Res. Bulletin*, 2000, **35**, 1869-1879.
3. K. S. Sohn, B. Cho and H. D. Park, *J. Am. Ceram. Soc.*, 1999, **82**, 2779-2784.
4. K. Omri and L. El Mir, *Superlattice Microst.*, 2014, **70**, 24-32.
5. Y. Q. Jiang, J. Chen, Z. X. Xie and L. S. Zheng, *Mater. Chem. Phys.*, 2010, **120**, 313-318.
6. Y. N. Xia, P. D. Yang, Y. G. Sun, Y. Y. Wu, B. Mayers, B. Gates, Y. D. Yin, F. Kim and Y. Q. Yan, *Adv. Mater.*, 2003, **15**, 353-389.
7. R. S. Devan, R. A. Patil, J. H. Lin and Y. R. Ma, *Adv. Funct. Mater.*, 2012, **22**, 3326-3370.
8. H. Q. Wang, G. H. Li, L. C. Jia, L. Li and G. Z. Wang, *Chem. Commun.*, 2009, **25**, 3786-3788.
9. Z. T. Kang, Y. Liu, B. K. Wagner, R. Gilstrap, M. Liu and C. J. Summers, *J. Lumin.*, 2006, **121**, 595-600.
10. X. F. Wang, H. T. Huang, B. Liu, B. Liang, C. Zhang, Q. Ji, D. Chen and G. Z. Shen, *J. Mater. Chem.*, 2012, **22**, 5330-5335.
11. M. Hafeez, A. Ali, S. Manzoor and A. S. Bhatti, *Nanoscale*, 2014, **6**, 14845-14855.
12. L. L. Wang, X. M. Liu, Z. Y. Hou, C. X. Li, P. P. Yang, Z. Y. Cheng, H. Z. Lian and J. Lin, *J. Phys. Chem. C*, 2008, **112**, 18882-18888.
13. S. Y. Zhang, M. Lu, Y. Li, F. Sun, J. C. Yang and S. L. Wang, *Mater. Lett.*, 2013, **100**, 89-92.
14. S. Y. Zhang, H. Y. Kang and Y. L. Gao, *Micro. Nano. Lett.*, 2014, **9**, 812-816.
15. J. S. An, J. H. Noh, I. S. Cho, H. S. Roh, J. Y. Kim, H. S. Han and K. S. Hong, *J. Phys. Chem. C*, 2010, **114**, 10330-10335.
16. S. Y. Zhang, L. L. Hou, M. H. Hou and H. J. Liang, *Mater. Lett.*, 2015, **156**, 82-85.
17. H. F. Wang, Y. Q. Ma, G. S. Yi and D. P. Chen, *Mater. Chem. Phys.*, 2003, **82**, 414-418.
18. H. Q. Wang, G. Z. Wang, L. C. Jia, C. J. Tang and G. H. Li, *J. Phys. Chem. C*, 2007, **111**, 14307-14311.
19. J. Zhou, J. Liu, X. D. Wang, J. H. Song, R. Tummala, N. S. Xu and Z. L. Wang, *Small*, 2007, **3**, 622-626.
20. J. Park, J. Kim and H. Kwon, *J. Korean Phys. Soc.*, 2017, **71**, 370-373.
21. C. S. Lewis, H. Q. Liu, J. Y. Han, L. Wang, S. Y. Yue, N. A. Brennan and S. S. Wong, *Nanoscale*, 2016, **8**, 2129-2142.
22. L. Wang, J. Han, Y. Zhu, R. Zhou, C. Jaye, H. Liu, Z.-Q. Li, G. T. Taylor, D. A. Fischer, J. Appenzeller and S. S. Wong, *J. Phys. Chem. C*, 2015, **119**, 26327-26338.
23. L. Wang, J. Han, B. Sundahl, S. Thornton, Y. Zhu, R. Zhou, C. Jaye, H. Liu, Z. Li, G. T. Taylor, D. A. Fischer, J. Appenzeller, R. J. Harrison and S. S. Wong, *Nanoscale*, 2016, **8**, 15553-15570.
24. J. Han, L. Wang and S. S. Wong, *J. Phys. Chem. C*, 2014, **118**, 5671-5682.
25. J. K. Han, L. Wang and S. S. Wong, *RSC Adv.*, 2014, **4**, 34963-34980.
26. J. Han, C. McBean, L. Wang, C. Jaye, H. Liu, D. A. Fischer and S. S. Wong, *J. Phys. Chem. C*, 2015, **119**, 3826-3842.
27. Y. Sun, R. Zou, Q. Tian, J. Wu, Z. Chen and J. Hu, *CrystEngComm*, 2011, **13**, 2273-2280.
28. I. Yonenaga, *Physica B*, 2001, **308**, 1150-1152.

29.   M. Adachi, Y. Murata, J. Takao, J. T. Jiu, M. Sakamoto and F. M. Wang, *J. Am. Chem. Soc.*, 2004, **126**, 14943-14949.
30.   L. Qu and X. Peng, *J. Am. Chem. Soc.*, 2002, **124**, 2049-2055.
31.   J. K. Han, C. McBean, L. Wang, J. Hoy, C. Jaye, H. Q. Liu, Z. Q. Li, M. Y. Sfeir, D. A. Fischer, G. T. Taylor, J. A. Misewich and S. S. Wong, *Chem. Mater.*, 2015, **27**, 778-792.
32.   K. A. Petrovykh, A. A. Rempel, V. S. Kortov and E. A. Buntov, *Inorg. Mater.*, 2015, **51**, 152-157.
33.   I. Maurin, G. Dantelle, J. P. Boilot and T. Gacoin, *J. Mater. Chem. C*, 2013, **1**, 13-22.
34.   Q. L. Dai, G. G. Zhang, P. Liu, J. Wang and J. K. Tang, *Inorg. Chem.*, 2012, **51**, 9232-9239.
35.   F. Wang, Y. Han, C. S. Lim, Y. H. Lu, J. Wang, J. Xu, H. Y. Chen, C. Zhang, M. H. Hong and X. G. Liu, *Nature*, 2010, **463**, 1061-1065.
36.   R. Saleh, N. F. Djaja and S. P. Prakoso, *J. Alloy Compd.*, 2013, **546**, 48-56.
37.   M. W. Wang, L. D. Sun, X. F. Fu, C. S. Liao and C. H. Yan, *Solid State Commun.*, 2000, **115**, 493-496.
38.   I. C. Masthoff, A. Gutsche, H. Nirschl and G. Garnweitner, *CrystEngComm*, 2015, **17**, 2464-2470.
39.   S. Y. Zhang, L. Ren and S. J. Peng, *CrystEngComm*, 2014, **16**, 6195-6202.
40.   A. Suino, S. Toyama, M. Takesue, H. Hayashi and R. L. Smith, *Mater. Chem. Phys.*, 2013, **137**, 1025-1030.
41.   C. Yoon and S. Kang, *J. Mater. Res.*, 2001, **16**, 1210-1216.
42.   R. Viswanatha, H. Amenitsch and D. D. Sarma, *J. Am. Chem. Soc.*, 2007, **129**, 4470-4475.
43.   P. K. Santra, S. Mukherjee and D. D. Sarma, *J. Phys. Chem. C*, 2010, **114**, 22113-22118.
44.   A. Degen and M. Kosec, *J. Eur. Ceram. Soc.*, 2000, **20**, 667-673.
45.   R. F. Egerton, *Physical principles of electron microscopy: an introduction to TEM, SEM and AEM*, Springer, New York, 2006.
46.   D. B. Williams and C. B. Carter, *Transmission electron microscopy : a textbook for materials science*, Springer, New York, 2008.
47.   M. Oku, K. Hirokawa and S. Ikeda, *J. Electron Spectrosc.*, 1975, **7**, 465-473.
48.   O. A. Bulavchenko, Z. S. Vinokurov, T. N. Afonasenko, P. G. Tsyrul'nikov, S. V. Tsybulya, A. A. Saraev and V. V. Kaichev, *Dalton Trans.*, 2015, **44**, 15499-15507.
49.   J. H. Li, D. Z. Shen, J. Y. Zhang, D. X. Zhao, B. S. Li, Y. M. Lu, Y. C. Liu and X. W. Fan, *J. Magn. Magn. Mater.,* 2006, **302**, 118-121.
50.   M. T. Tsai, Y. H. Lin and J. R. Yang, *Iop Conf. Ser. Mat. Sci.*, 2011, **18**, 032026/1-5.
51.   N. F. Samsudin, K. A. Matori, J. Y. C. Liew, Y. W. Fen, M. H. M. Zaid and Z. N. Alassan, *J. Spectrosc.*, 2015, **2015**, 730753/1-7.
52.   M. Takesue, H. Hayashi and R. L. Smith, *Prog. Cryst. Growth Ch.*, 2009, **55**, 98-124.
53.   K. H. Yoon and J. H. Kim, *J. Korean Phys. Soc.*, 2011, **58**, 1668-1671.
54.   L. Dacanin, S. R. Lukic, D. M. Petrovic, Z. Antic, R. Krsmanovic, M. Marinovic-Cincovic and M. D. Dramicanin, *J. Mater. Eng. Perform.*, 2012, **21**, 1509-1513.
55.   H. S. Roh, Y. C. Kang, C. H. Lee, H. D. Park and S. B. Park, *Jpn J. Appl. Phys. 1ett.*, 2003, **42**, 3429-3433.
56.   S. F. Wang, M. K. Lu, F. Gu, Y. X. Qi, D. Xu, D. R. Yuan and D. X. Cao, *Appl. Phys. a-Mater.*, 2005, **80**, 871-874.
57.   V. Sivakumar and A. Lakshmanan, *J. Lumin.*, 2014, **145**, 420-424.

58.   K. Omri, A. Alyamani and L. E. Mir, *Appl. Phys. A*, 2018, **124**, 215/1-7.
59.   D. J. Robbins, E. E. Mendez, E. A. Giess and I. F. Chang, *J. Electrochem. Soc.*, 1984, **131**, 141-146.
60.   Z. C. Wei, Z. F. Wang, W. R. T. Tait, M. Pokhrel, Y. B. Mao, J. J. Liu, L. C. Zhang, W. X. Wang and L. Y. Sun, *J. Mater. Sci.*, 2018, **53**, 1824-1832.
61.   S. H. Linwood and W. A. Weyl, *J. Opt. Soc. Am.*, 1942, **32**, 443-453.
62.   H. C. Lin, P. Xie, Y. Liu, X. Zhou and B. J. Li, *Nanotechnology*, 2015, **26**, 335401/1-9.
63.   R. S. Swathi and K. L. Sebastian, *J. Chem. Phys.*, 2009, **130**, 086101/1-6.
64.   L. Gaudreau, K. J. Tielrooij, G. E. D. K. Prawiroatmodjo, J. Osmond, F. J. G. de Abajo and F. H. L. Koppens, *Nano. Lett.*, 2013, **13**, 2030-2035.
65.   F. Federspiel, G. Froehlicher, M. Nasilowski, S. Pedetti, A. Mahmood, B. Doudin, S. Park, J. O. Lee, D. Halley, B. Dubertret, P. Gilliot and S. Berciaud, *Nano. Lett.*, 2015, **15**, 1252-1258.
66.   H. Y. Chen, S. Maiti and D. H. Son, *ACS Nano*, 2012, **6**, 583-591.
67.   S. Joicy, R. Saravanan, D. Prabhu, N. Ponpandian and P. Thangadurai, *RSC Adv.*, 2014, **4**, 44592-44599.
68.   T. Debnath, S. Maiti and H. N. Ghosh, *J. Phys. Chem. Lett.*, 2016, **7**, 1359-1367.
69.   H. Chang, H. D. Park, K. S. Sohn and J. D. Lee, *J. Korean Phys. Soc.*, 1999, **34**, 545-548.

TOC entry: Charge transfer and energy transfer phenomena were observed and analyzed in heterostructure systems comprised of CdSe QDs immobilized onto Mn-doped Zn_2SiO_4 nanowire host materials.